

Carbon Isotope Fractionation of Complex Organic Molecules in Star-Forming Cores

RYOTA ICHIMURA ^{1,2}, HIDEKO NOMURA ^{1,2} AND KENJI FURUYA ^{1,3}

¹*Division of Science, National Astronomical Observatory of Japan, 2-21-1 Osawa, Mitaka, Tokyo 181-8588, Japan*

²*Department of Astronomical Science, The Graduate University for Advanced Studies, SOKENDAI, 2-21-1 Osawa, Mitaka, Tokyo 181-8588, Japan*

³*Department of Astronomy, Graduate School of Science, University of Tokyo, Tokyo 113-0033, Japan*

ABSTRACT

Recent high-resolution and sensitivity ALMA observations have unveiled the carbon isotope ratios ($^{12}\text{C}/^{13}\text{C}$) of Complex Organic Molecules (COMs) in a low-mass protostellar source. To understand the $^{12}\text{C}/^{13}\text{C}$ ratios of COMs, we investigated the carbon isotope fractionation of COMs from prestellar cores to protostellar cores with a gas-grain chemical network model. We confirmed that the $^{12}\text{C}/^{13}\text{C}$ ratios of small molecules are bimodal in the prestellar phase: CO and species formed from CO (e.g., CH_3OH) are slightly enriched in ^{13}C compared to the local ISM (by $\sim 10\%$), while those from C and C^+ are depleted in ^{13}C owing to isotope exchange reactions. COMs are mainly formed on the grain surface and in the hot gas ($> 100\text{ K}$) in the protostellar phase. The $^{12}\text{C}/^{13}\text{C}$ ratios of COMs depend on which molecules the COMs are formed from. In our base model, some COMs in the hot gas are depleted in ^{13}C compared to the observations. Thus, We additionally incorporate reactions between gaseous atomic C and H_2O ice or CO ice on the grain surface to form H_2CO ice or C_2O ice, as suggested by recent laboratory studies. The direct C-atom addition reactions open pathways to form ^{13}C -enriched COMs from atomic C and CO ice. We find that these direct C-atom addition reactions mitigate ^{13}C -depletion of COMs, and the model with the direct C-atom addition reactions better reproduces the observations than our base model. We also discuss the impact of the cosmic ray ionization rate on the $^{12}\text{C}/^{13}\text{C}$ ratio of COMs.

Keywords: astrochemistry — ISM:molecules — molecular processes

1. INTRODUCTION

In the central ($< 100\text{ AU}$) and hot ($> 100\text{ K}$) regions in low-mass protostellar cores, rotational transition lines from various species have been observed. Some species are referred to as complex organic molecules (COMs), defined as organic molecules with six or more atoms (Herbst & van Dishoeck 2009).

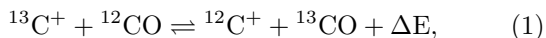
According to astrochemical models, the formation of COMs requires a sequence of grain surface processes during star formation. This includes freeze-out of gaseous species onto the grain surface, and grain surface chemistry at low temperature ($\sim 10\text{ K}$) to produce simple icy molecules such as CH_4 and CH_3OH . After protostar formation, the gas and dust temperatures increase (above

$\sim 25\text{ K}$), radicals form and COMs are produced via radical-radical reactions on the grain surface via diffusion (e.g., Garrod & Herbst 2006; Herbst & van Dishoeck 2009). Additionally, recent laboratory experiments suggest that the atomic C insertion or addition reaction on the grain surface may be important for the production of the COMs and increasing their complexity (Tsuge et al. 2023; Ferrero et al. 2024). Also, nondiffusive grain surface chemistry may be important for the formation of COMs under low-temperature conditions (Shingledecker et al. 2018; Jin & Garrod 2020; Garrod et al. 2022). However, it is still challenging to reveal the formation pathways of COMs.

The measurement of isotope ratios and their fractionation is useful to investigate the local chemical process such as the formation pathways of COMs in star-forming regions. Carbon isotope ratio of different COMs has been measured with high-resolution ALMA observations

towards the Class 0 low-mass protostellar binary system IRAS 16293-2422. The values were found to be comparable with the local ISM value ($^{12}\text{C}/^{13}\text{C} = 68$; Milam et al. 2005) or to show lower $^{12}\text{C}/^{13}\text{C}$ ratios towards source B (Jørgensen et al. 2016, 2018), while are consistent within the error with the local ISM value for source A (Manigand et al. 2020). In the Class I low-mass young outbursting star V883 Ori, COMs are enriched in ^{13}C ($^{12}\text{C}/^{13}\text{C} \sim 20\text{-}30$) (Yamato et al. 2024).

Carbon isotope fractionation in the ISM is thought to occur via exothermic isotope exchange reactions, isotope selective photodissociation, and desorption from grain surface with the different binding energies of isotopologues (Nomura et al. 2023). Especially, several studies of astrochemical models focus on exothermic isotope exchange reactions to reproduce the observed carbon isotope ratios of fractionated simple molecules (e.g. $\text{C}_2\text{H}/^{13}\text{CCH} > 250$ and $\text{HC}_3\text{N}/\text{H}^{13}\text{CCCN} = 79$) in dense interstellar clouds (Langer et al. 1984; Furuya et al. 2011; Roueff et al. 2015; Colzi et al. 2020; Loison et al. 2020; Sipilä et al. 2023). Isotope exchange reactions can fractionate carbon-bearing species because of the zero-point vibrational energy difference between ^{13}C isotopologues and ^{12}C isotopologues. One of the most important carbon isotope exchange reactions is



where the vibrational energy difference is $\Delta E = 35$ K (Watson et al. 1976). Langer et al. (1984) have introduced this exchange reaction into their gas-phase astrochemical model. They concluded that at a low temperature (~ 20 K), the forward reaction of the reaction in Eq.(1) is efficient compared to the backward reaction, and the small carbon-bearing species are divided into two groups; ^{13}C -rich species formed from CO (e.g., CO_2 and CH_3OH) and ^{13}C -poor species formed from C^+ (e.g., CH_4). In addition to the reaction in Eq.(1), other carbon isotope exchange reactions have been suggested based on quantum chemical calculations such as $^{13}\text{C} + \text{C}_3 \rightleftharpoons ^{12}\text{C} + ^{13}\text{CC}_2 + 28$ K and lead to carbon isotope fractionation (Roueff et al. 2015; Colzi et al. 2020; Loison et al. 2020).

Isotope selective photodissociation and the difference in binding energies among different isotopologues also cause carbon isotope fractionation. For example, self-shielding of CO against UV photodissociation can cause the fractionation (van Dishoeck & Black 1988; Visser et al. 2009). This effect is however only pronounced at visual extinction of $A_v \sim 1$ mag. Moreover, ^{12}CO have a slightly lower binding energy than ^{13}CO because it is lighter (Smith et al. 2015, 2021). Consequently, carbon-bearing species in the solid phase may be en-

riched in ^{13}C , while those in the gas phase may be depleted in ^{13}C . Jørgensen et al. (2016, 2018) suggested that the observed carbon isotope fractionation of COMs in IRAS16293-2422B might be affected by isotope selective photodissociation of CO and/or difference in binding energies between ^{12}CO and ^{13}CO .

Furuya et al. (2011); Colzi et al. (2020); Loison et al. (2020); Sipilä et al. (2023) studied carbon isotope fractionation of some simple molecules such as C_2H and HCN and HC_3N using the astrochemical model in prestellar cores with 10K. Meanwhile, Garrod (2013); Aikawa et al. (2008) studied the formation of COMs using astrochemical models in low- and high-mass star-forming cores with temperatures up to around 200K.

In this paper, we report gas-grain chemical reaction network calculations, systematically investigating the carbon isotope fractionations of COMs. This calculation includes their formation before star formation and their sublimation into the gas phase following star formation. In section 2, we describe a physical model of a star-forming core and the gas-grain chemical model. In Section 3, we present the results of time variation of molecular abundances and $^{12}\text{C}/^{13}\text{C}$ ratios in the base model. The effects of the atomic C insertion or addition reactions on the grain surface and difference in binding energy between ^{12}CO and ^{13}CO and the initial condition of carbon and $^{12}\text{C}/^{13}\text{C}$ ratio of C^+ are also studied. In Section 4, we compare our calculation results with the observations in the IRAS 16293-2422B source. We also discuss the effect of cosmic ray (CR) ionization rates on $^{12}\text{C}/^{13}\text{C}$ ratios of COMs. Our findings are summarized in Section 5.

2. MODEL

2.1. Physical Model

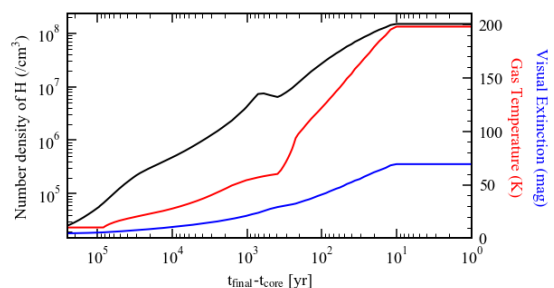


Figure 1. Temporal variation of the number density of hydrogen nuclei (black line), gas temperature (red line), and visual extinction (blue line) of a fluid parcel along a streamline in a gravitationally collapsing core.

We adopt one-dimensional radiation hydrodynamics simulations by Masunaga & Inutsuka (2000) as a phys-

ical model. This model traces the evolution of a dense, starless core to a protostellar core. A fluid parcel is traced in the hydrodynamics simulation, and we calculate the evolution of molecular abundances with a chemical reaction network along the fluid parcel as done in Aikawa et al. (2008, 2020). The model is divided into two phases: the static phase and the collapse phase. In the static phase, the prestellar core is in hydrostatic equilibrium assuming that turbulence prevents the contraction of the core. In the calculations, we adopt the gas and dust temperature of 10 K, the number density of hydrogen nuclei of $2.28 \times 10^4 \text{ cm}^{-3}$, and the visual extinction of 4.51 mag, which correspond to the value of the fluid parcel at 1×10^4 au from the core center (Masunaga & Inutsuka 2000; Aikawa et al. 2008). In the subsequent collapse phase, a protostar is formed due to gravitational collapse and further grows through envelope accretion. Following the first collapse and the formation of an adiabatic core, the protostar is born at 2.5×10^5 yr when the second collapse stops (Masunaga & Inutsuka 2000; Aikawa et al. 2008). This model further proceeds to track the physical evolution for 9.3×10^4 yr until the fluid parcel reaches 30.6 au from the core center. Figure 1 shows the temporal variation of the number density of hydrogen nuclei, gas temperature, and visual extinction in a fluid parcel. We define the moment of the protostar formation as $t_{\text{core}} = 0$ and the end of calculation as $t_{\text{core}} = t_{\text{final}} = 9.3 \times 10^4$ yr. To increase the visibility of the evolution around the final stage, we adjust the horizontal axis to the logarithmic scale of $t_{\text{final}} - t_{\text{core}}$ (Aikawa et al. 2008). At $t_{\text{core}} = t_{\text{final}}$ in the collapse phase, which is the final time step with both gas and dust temperatures reaching ~ 198 K, the total H_2 density reaching $\sim 1.49 \times 10^8 \text{ cm}^{-3}$, and visual extinction ~ 70 mag. The infalling timescale inside 1000 au is shorter than the lifetime of the protostar in this model so that we can use the time evolution of abundances in a single fluid parcel to represent the true radial distribution (Aikawa et al. 2020). For the sake of simplicity, we set a minimum temperature of 10 K throughout our simulations.

2.2. Chemical Model

2.2.1. The base model

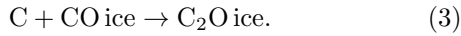
We utilize the gas-ice astrochemical code based on the rate equation approach (Rokko code; Furuya et al. 2015) and incorporate two hydrogenation reactions on grain surface; $\text{CH}_2\text{CO ice} + \text{H ice} \rightarrow \text{CH}_3\text{CO ice}$ and $\text{CH}_3\text{CO ice} + \text{H ice} \rightarrow \text{CH}_3\text{CHO}$ (Ruaud et al. 2015). We also expand to include mono- ^{13}C species and carbon isotope exchange reactions (see Table A1). The chemistry is described by a three-phase model (Furuya et al. 2016).

This model makes a distinction between the surface of the ice mantle and the rest of the ice mantle (Hasegawa & Herbst 1993). Like in Hasegawa & Herbst (1993), we assume that the ice mantle phase remains chemically inert, while the ice surface phase considers chemical reactions. Species in our chemical network consist of carbon skeletons up to three carbons to reduce computational time. We consider the species with a different position of ^{13}C as the same species (e.g., $^{12}\text{C}^{13}\text{CH}$ and $^{13}\text{C}^{12}\text{CH}$ are the same species) for simplicity. We have omitted the multiple fractionations, such as two or more ^{13}C for simplicity. Isotope exchange reactions are taken from Roueff et al. (2015) and Loison et al. (2020), and they are considered in the gas phase. ^{13}C -bearing species, however, are taken into account in ice surface chemistry through the adsorption of ^{13}C -bearing species onto the grain surface and the subsequent grain surface reactions, such as hydrogenation of species. We neglect ^{13}C fractionation via the isotope selective photodissociation in the following sections because we only consider the dense region. Our reaction network consists of 733 gas and grain species and 20360 gas phase and grain surface reactions.

We assume the Langmuir-Hinshelwood mechanism to describe two-body reactions on grain surfaces. In this mechanism, species on the grain surface diffuse by thermal hopping and react with each other when they meet. The set of adsorption energies is adopted from Furuya et al. (2015). The barrier for thermal diffusion of atoms and molecules, excluding hydrogen (H), is set to be 40 % of the adsorption energy (E_{des}). The barrier is set at 30 % of E_{des} for hydrogen. We assume that the sticking probability of colliding gaseous species except for hydrogen onto the grain is unity. For hydrogen, the sticking probability is calculated based on Hollenbach & McKee (1979). We adopt the low-metal elemental abundances taken from Aikawa et al. (2001) through our calculations. The species are assumed to be initially atoms or atomic ions, except for hydrogen, which is in H_2 . The dust grain is spherical with a $0.1 \mu\text{m}$ radius with the material density of 2.5 g/cm^3 . The dust-to-gas ratio is set to 0.01. The CR ionization rate of H_2 is set to be $1.3 \times 10^{-17} \text{ s}^{-1}$ (Terzieva & Herbst 1998). In this paper, we define "abundance" as the fractional abundance of species to hydrogen nuclei. $^{12}\text{C}/^{13}\text{C}$ ratios are measured by the statistical factor corresponding to the two or three indistinguishable carbon atoms. For example, C_2H has two kinds of carbon isotopologues of $^{13}\text{C}^{12}\text{CH}$ and $^{12}\text{C}^{13}\text{CH}$, but they are not distinguished in our chemical reaction network. Therefore, the $^{12}\text{C}/^{13}\text{C}$ ratio of C_2H is calculated as ' $n(\text{C}_2\text{H})/n(^{13}\text{C}\text{-containing } \text{C}_2\text{H})$ ' multiplied by 2 in this work.

2.2.2. The direct C-atom addition reactions

Besides the Langmuir-Hinshelwood process, complex molecules could be formed via nondiffusive grain surface reactions at low temperature (Jin & Garrod 2020; Garrod et al. 2022). Given atomic carbon’s high binding energy of 10,000 K, its diffusion on grain surfaces at the low temperatures of the ISM is challenging. However, recent laboratory experiments and quantum chemical calculations reveal that atomic C reacts with icy light species (e.g., H₂O, and CO) to form H₂CO and C₂O ice on the grain surface at 10K, respectively (Molpeceres et al. 2021; Fedoseev et al. 2022; Ferrero et al. 2023). Under ISM condition, H₂O and CO, with binding energies of 5,600K and 833K respectively, show slow diffusion on the grain surface. Therefore, we characterize the low-temperature reactions involving atomic C with H₂O and CO chemistries as Eley-Rideal (ER) reactions, which are the direct collision of a gaseous species with adsorbed species on a grain surface. We incorporate the subsequent two ER reactions involving atomic C (hereafter direct C-atom addition reaction) into the model presented in Section 3.2.



These direct C-atom addition reactions are assumed to occur when atomic C is adsorbed from the gas phase onto its reaction partner on the grain surface. Therefore, the reaction coefficient (s⁻¹) of the direct C-atom addition reaction (k_{Cadd}) is given by

$$k_{Cadd} = A \times k_{acc} \times \frac{n_s(X)}{n_s(total)}, \quad (4)$$

$$k_{acc} = n_{grain} S \sigma \langle v \rangle, \quad (5)$$

k_{acc} is the accretion rate coefficient of atomic C onto a grain surface. n_{grain} is the number density of dust grains, S is the sticking probability, σ is the geometrical cross-section of a dust grain, $\langle v \rangle$ is the thermal velocity of atomic C, and $n_s(X)$ is the number density of species X on a grain surface. For Eq.(4), $n_s(total)$ is the number density of total species present on a grain surface, and A is a branching ratio. According to quantum chemical calculations, for the reaction in Eq.(2), approximately 30% of adsorbed atomic C on H₂O converts to H₂CO via a barrierless pathway, while the remaining atomic C is present as it is (Molpeceres et al. 2021; Tsuge et al. 2023), so the branching ratio of the reaction in Eq.(2) is set to be 0.3 ($A = 0.3$). For the reaction in Eq.(3), all

adsorbed atomic C on CO converts to C₂O in a barrierless way (Ferrero et al. 2023), so the branching ratio is set to be 1 ($A = 1.0$). Some gaseous atomic C take part in these direct C-atom addition reactions instead of the adsorption, so the adsorption rate coefficient of atomic C is adjusted by subtracting the rate coefficient of the direct C-atom addition reaction as

$$k_{acc,adj} = k_{acc} - k_{Cadd}, \quad (6)$$

where $k_{acc,adj}$ is the adjusted accretion rate coefficient. The impact of direct C-atom addition reactions on the ¹²C/¹³C ratios of COMs is discussed in Sect. 3.2.

3. RESULTS

3.1. The Base Model

3.1.1. The Static Phase

Figure 2 shows the temporal variation of abundances and ¹²C/¹³C ratios of some selected species in the static phase with a fixed temperature (10 K), density ($2.28 \times 10^4 \text{ cm}^{-3}$) and CR ionization rate ($1.3 \times 10^{-17} \text{ s}^{-1}$). With the exception of considering different positions for ¹³C or differences in the number of isotope exchange reactions the models in Colzi et al. (2020) and Loison et al. (2020) are similar to our model in the static phase. Nitrogen-bearing species related to isotope exchange reactions are discussed in Appendix B.2. Dominant carriers of carbon in the gas phase change as time goes on. Initially, C⁺ is dominant. C⁺ is gradually converted to atomic C and then to CO at $\sim 10^5 \text{ yr}$. These small gas-phase species freeze out onto the grain surface and contribute to surface reactions. Adsorbed atomic C is converted to CH₄ ice via a sequence of hydrogenation reactions on the grain surfaces before 10^5 yr , while adsorbed CO is converted to CH₃OH ice. During the static phase, ¹³C fractionation occurs via isotope exchange reactions (Furuya et al. 2011; Colzi et al. 2020; Loison et al. 2020). For example, considering ¹³C⁺ + ¹²CO \rightleftharpoons ¹²C⁺ + ¹³CO + 35 K (Eq.(1)) or ¹³C + C₃ \rightleftharpoons ¹²C + ¹³CC₂ + 28 K, these isotope exchange reactions lead to the depletion of ¹³C in atomic C and C⁺, while CO and C₃ become enriched in ¹³C until $1 \times 10^5 \text{ yr}$. Around $2 \times 10^5 \text{ yr}$, CO becomes the dominant carrier of gas-phase carbon, so the ¹²C/¹³C ratio of CO gets closer to the local ISM value (Furuya et al. 2011). The abundance of gaseous atomic C decreases with time due to the conversion to CO and CH₄ ice. Around $2 \times 10^5 \text{ yr}$, gaseous atomic C is produced from C₃ and C₂ via photodissociation or reaction with atomic O. Therefore, the ¹²C/¹³C ratio of atomic C temporally approaches to the local ISM value due to the low ¹²C/¹³C ratio of C₃ and C₂. After that, C⁺, which is produced through

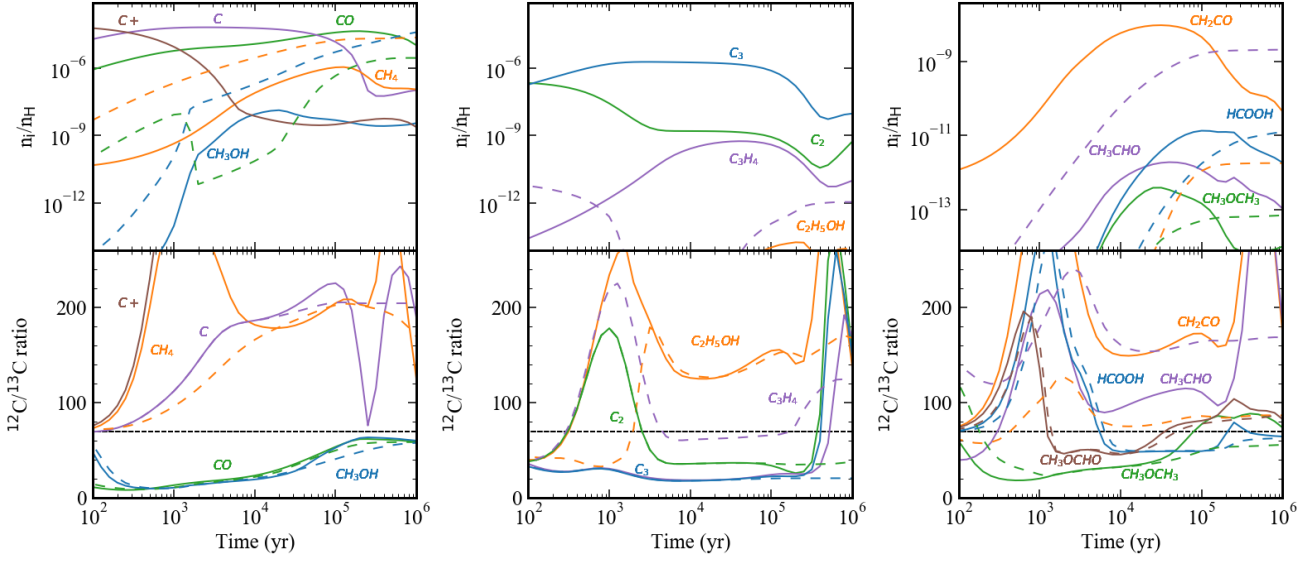


Figure 2. Temporal variation of the molecular abundances and $^{12}\text{C}/^{13}\text{C}$ ratios for gaseous species (solid lines) and icy species (dashed lines) during the static phase in the base model. The horizontal black dashed line represents the average $^{12}\text{C}/^{13}\text{C}$ ratio of local ISM.

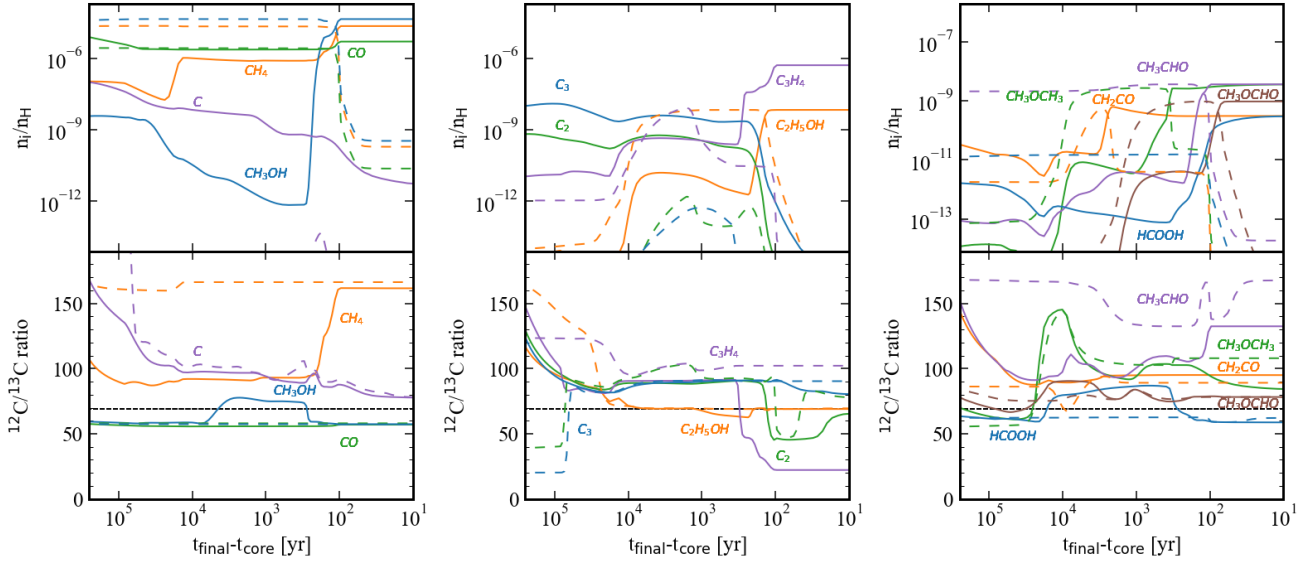


Figure 3. Same as Figure 2 but during the collapse phase.

the destruction of CO by He^+ , is converted to gaseous atomic C or C_3 , so these species become depleted in ^{13}C . Around 10^3 yr, some species such as C_2 are depleted in ^{13}C as they are formed from C^+ or atomic C, and after that they are enriched in ^{13}C since their major reactants change into ^{13}C -enriched C_3 or CO.

Icy molecules (e.g. CH_4 and CH_3OH) are formed via adsorption of these fractionated small species (e.g. CO or atomic C) and surface reactions, and thus the time variation of $^{12}\text{C}/^{13}\text{C}$ ratios of the icy molecules follow those of gas-phase species. For example, before 10^5 yr,

icy molecules such as CH_4 and CH_3OH are formed from atomic C and CO, therefore the $^{12}\text{C}/^{13}\text{C}$ ratios of these icy molecules reflect the ratios of atomic C or CO. After 10^5 yr when CO becomes the main carbon reservoir, the carbon isotope ratio of CH_3OH ice becomes closer to the local ISM value, reflecting that of CO in the gas phase. Meanwhile, the formation of CH_4 ice becomes negligible since most atomic C is converted to CO after 10^5 yr. Therefore, CH_4 ice keeps the high carbon isotope ratio in the same as before 10^5 yr. Consequently, the $^{12}\text{C}/^{13}\text{C}$ ratios of dominant icy molecules exhibit a bimodal pro-

file: depletion of ^{13}C or similar to or slightly enriched in ^{13}C (by $\sim 10\%$) compared to the local ISM value.

COMs are formed from simple molecules. Before around 10^5 yr when C^+ and atomic C are the main carbon reservoir, COMs (e.g. CH_3CHO) and their ices are mainly formed from ^{13}C -poor molecules, while after around 10^5 yr when CO is main carbon reservoir, COMs (e.g. CH_3OCH_3) and their ice are formed from slightly ^{13}C -rich CO or CH_3OH on the grain surface or adsorbed on grains after the formation in the gas phase. The $^{12}\text{C}/^{13}\text{C}$ ratios of COMs follow those of simple molecules and exhibit a bimodal profile. Some molecules including COMs (e.g. CH_3OCHO and HCOOH) are formed from both ^{13}C -poor species and ^{13}C -rich species. For example, CH_3OCHO is formed from H_2CO . H_2CO is formed from CO ice on the grain surface and CH_3 in the gas phase, so the $^{12}\text{C}/^{13}\text{C}$ ratios of these molecules including COMs show the intermediate value between the bimodal profile.

3.1.2. The Collapse Phase

In the collapse phase (see Fig.1), icy molecules on the grain surface sublime into the gas phase at their sublimation temperatures, which depend on their binding energies, and the rest in the bulk ice mantle are trapped in water ice and sublime at ~ 120 K together with water ice. Moreover, some species are additionally produced by grain surface reactions. Figure 3 shows the temporal variation of abundances and $^{12}\text{C}/^{13}\text{C}$ ratios of selected species in the collapse phase. For CH_4 , the binding energy is set to be 1300 K, CH_4 ice on the surface sublimates around 20 K ($t_{\text{final}} - t_{\text{core}} \sim 2 \times 10^4$ yr) and the gas phase CH_4 abundance increases to almost 1×10^{-6} . After that, whole CH_4 ice sublimates at ~ 120 K ($t_{\text{final}} - t_{\text{core}} \sim 10^2$ yr) together with water ice. The $^{12}\text{C}/^{13}\text{C}$ ratios of abundant molecules (molecular abundance of $\sim 10^{-5}$) molecules such as CH_4 and CH_3OH after water ice sublimation ($t_{\text{final}} - t_{\text{core}} \sim 10^2$ yr) reflect those of ice formed during the static phase. After water ice sublimates at ~ 120 K, the $^{12}\text{C}/^{13}\text{C}$ ratio of sublimated CH_4 becomes significantly depleted in ^{13}C as well as that of CH_4 ice while that of sublimated CH_3OH becomes enriched in ^{13}C as well as that of CH_3OH ice.

On the other hand, some icy COMs (e.g. CH_3CHO and CH_3OCHO) are produced via radical-radical reactions on the grain surface during the collapse phase. The abundances of the additionally formed ices are equivalent to or exceeding the abundances of the icy COMs formed during the static phase. Therefore, the $^{12}\text{C}/^{13}\text{C}$ ratios of some sublimated COMs (e.g. CH_3CHO and CH_3OCHO) are different from those of their ice formed in the static phase. The $^{12}\text{C}/^{13}\text{C}$ ratios of icy molecules

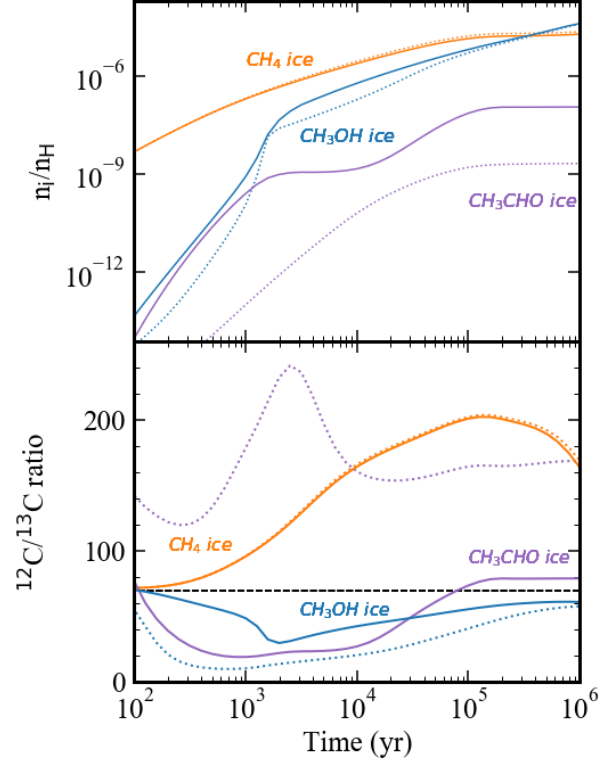


Figure 4. Temporal variation of the molecular abundances and $^{12}\text{C}/^{13}\text{C}$ ratios of CH_4 ice, CH_3OH ice, and CH_3CHO ice during the static phase for the base model (dotted lines) and the model with the direct C-atom addition reactions (solid lines).

formed during the collapse phase depend on the $^{12}\text{C}/^{13}\text{C}$ ratios of reactants such as radicals. For example, the CH_3OCHO ice is formed from ^{13}C -enriched HCO radical ($^{12}\text{C}/^{13}\text{C} \sim 30$) during the collapse phase, so the $^{12}\text{C}/^{13}\text{C}$ ratio of CH_3OCHO ice decreases, and eventually the $^{12}\text{C}/^{13}\text{C}$ ratio of sublimated CH_3OCHO is different from that of ice formed in the static phase. Consequently, the $^{12}\text{C}/^{13}\text{C}$ ratios of some COMs after water ice sublimation are essentially a mixture of those formed during the static phase and the collapse phase, sometimes closer to the $^{12}\text{C}/^{13}\text{C}$ ratios of icy COMs formed during the collapse phase rather than those in the static phase. Moreover, the formation of a part of COMs proceeds even in the gas phase via ion-neutral reactions after the sublimation, resulting in distinct carbon isotope ratios compared to those in ice before sublimation. The detailed explanation for other complex molecules is presented in Section 4.1.

3.2. The effect of the direct C-atom addition reactions

Based on recent laboratory experiments and quantum chemical calculations, we incorporate the two direct C-atom addition reactions by the ER mechanism; Eq.(2)

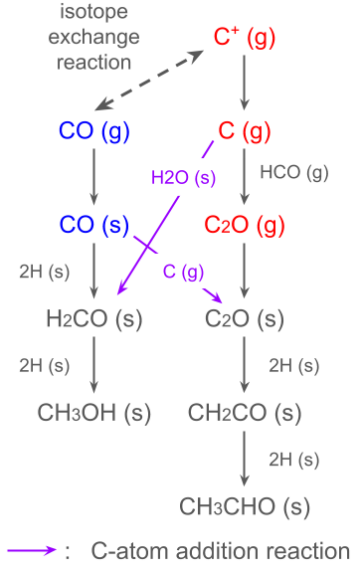


Figure 5. Schematic formation pathways of CH_3OH and CH_3CHO with the direct C-atom addition reaction. Gas phase species (g) link to the icy species on the grain surface (s). The dashed arrow indicates the isotope exchange reaction. Red-colored species are depleted in ^{13}C , while blue-colored species are enriched in ^{13}C . Purple arrows indicate the direct C-atom addition reaction. Species 2H indicate consecutive hydrogenation reactions on the grain surfaces.

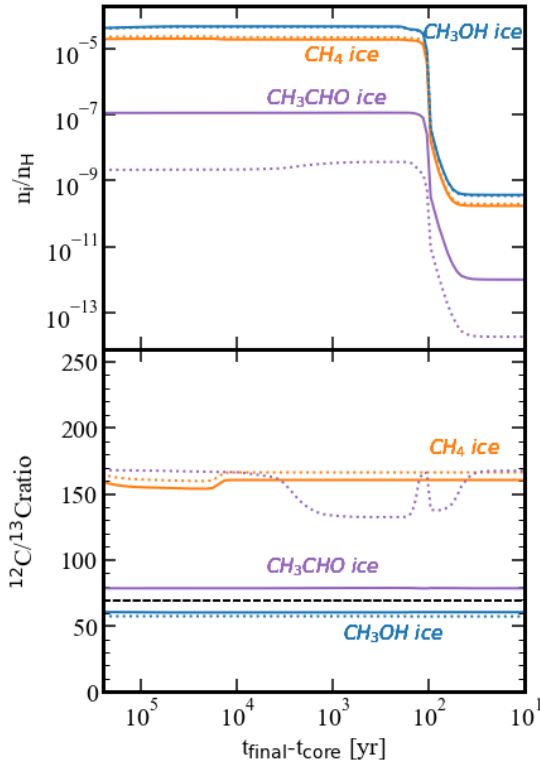


Figure 6. Same as Figure 4 but during the collapse phase.

(Molpeceres et al. 2021; Potapov et al. 2021) and Eq.(3) (Fedoseev et al. 2022). Figure 4 shows the temporal variation of abundances and $^{12}\text{C}/^{13}\text{C}$ ratios of some icy species in the static phase without and with the direct C-atom addition reactions. In the model with the direct C-atom addition reactions, the abundances of icy CH_3OH and CH_3CHO increase compared to the base model. On the other hand, the abundance of CH_4 ice, which is mainly formed via hydrogenation reactions of atomic C on the grain surfaces, slightly decreases compared to the base model (by $\sim 15\%$). The $^{12}\text{C}/^{13}\text{C}$ ratios of icy CH_3OH and CH_3CHO in the model with the direct C-atom addition reactions are closer to the ISM value compared to those in the base model. CH_3OH ice is formed via hydrogenation reactions of ^{13}C -enriched CO ice on the grain surfaces in the base model. In contrast, in the direct C-atom addition model CH_3OH ice is additionally formed from slightly ^{13}C -depleted atomic C via the reaction in Eq.(2) and the subsequent hydrogenation reactions on the grain surfaces. CH_3CHO ice is formed from ^{13}C -depleted C^+ and atomic C via gas-phase reaction with HCO and the subsequent hydrogenation reactions on grain surfaces in the base model. In contrast, in the model with the direct C-atom addition reactions CH_3CHO ice is additionally formed from slightly ^{13}C -depleted atomic C and ^{13}C -enriched CO via the reaction in Eq.(3) followed by a sequence of hydrogenation reactions on the grain surfaces. These formation processes make differences in carbon isotope ratios of CH_3OH and CH_3CHO between the models with and without the direct C-atom addition reactions.

Figure 5 shows formation pathways of CH_3OH and CH_3CHO in the models with the direct C-atom addition reactions which suggests that due to these reactions, the isotope ratios of some species could change. Figure 6 shows the temporal variation of abundances and $^{12}\text{C}/^{13}\text{C}$ ratios of some icy species in the collapse phase without and with the direct C-atom addition reactions. Some icy complex molecules related to the direct C-atom addition reactions (e.g. CH_3CHO) have lower $^{12}\text{C}/^{13}\text{C}$ ratios compared to those in the base model. After water ice sublimation, molecules that are formed via the direct C-atom addition reactions and following reactions, also have lower $^{12}\text{C}/^{13}\text{C}$ ratios compared to those in the base model (see Figure 9). We note that Molpeceres et al. (2021) treated water clusters as the representative ice on grain surfaces, so variations in the composition of interstellar ice could affect the branching ratio A . Therefore, we additionally run models changing the branching ratio A , and find that the results obtained with $A = 0.15$ are consistent with those derived when A is set to 0.3. We discuss the effect of the direct C-atom

addition reactions for selected individual species in Section 4.1 and we show the results of the model with the direct C-atom addition reactions in Section B.

3.3. The effect of the difference in Binding Energy between ^{12}CO and ^{13}CO

If the binding energies of CO isotopologues on the dust surface are mass-dependent and thus ^{13}CO is larger than that of ^{12}CO , ^{12}CO can sublimate at a lower temperature than ^{13}CO . Consequently, CO in the gas phase would become depleted in ^{13}C , while CO ice would become enriched in ^{13}C . Smith et al. (2015) theoretically investigated the mass-dependence of thermal desorption of CO and dust temperature for segregation between ^{12}CO and ^{13}CO in the ices. They considered the balance between the adsorption rates and desorption rates for $^{12}\text{C}^{16}\text{O}$ and $^{13}\text{C}^{16}\text{O}$. As a result, assuming a 10 K difference in binding energy, the $^{12}\text{CO}/^{13}\text{CO}$ gas ratio reaches twice as high as the elemental $^{12}\text{C}/^{13}\text{C}$ ratio at a gas temperature of 10 K. Moreover, Smith et al. (2021) derived binding energies of pure ^{12}CO ice and pure ^{13}CO ice to be 833 ± 5 K, and 846 ± 6 K respectively based on laboratory experiments. We additionally run models assuming that the binding energy of ^{12}CO is 833 K and that of ^{13}CO is 846 K for both the static phase and the collapse phase. We find that the difference in binding energy does not affect the $^{12}\text{C}/^{13}\text{C}$ ratios of COMs although the difference leads to the desorption rate of CO to be slightly increased, nearly 10 %.

3.4. Dependence on the elemental $^{12}\text{C}/^{13}\text{C}$ ratio and Initial Condition of Carbon

In our models presented in the previous section, we assume the elemental $^{12}\text{C}/^{13}\text{C}$ ratio is 68, which corresponds to the local ISM value (Milam et al. 2005). Here, we explore how our results depend on the assumed value of the elemental $^{12}\text{C}/^{13}\text{C}$ ratio. Figure 7 shows the temporal variation in the collapse phase with the elemental $^{12}\text{C}/^{13}\text{C}$ ratio = 89 which is the average value in the Solar System. We find that the $^{12}\text{C}/^{13}\text{C}$ ratios of molecules are scaled with assumed $^{12}\text{C}/^{13}\text{C}$ ratio.

So far we assumed that carbon is initially present as $^{12}\text{C}^+$ and $^{13}\text{C}^+$. Here, we investigate the dependence of the initial form of carbon on the carbon isotope ratios of molecules. We additionally run models with and without the direct C-atom addition reactions during the static phase and collapse phase where initially half of the carbon is present as ^{12}CO and ^{13}CO with $^{12}\text{CO}/^{13}\text{CO} = 68$, while the rest is present as $^{12}\text{C}^+$ and $^{13}\text{C}^+$ with $^{12}\text{C}^+/^{13}\text{C}^+ = 68$. Figure 8 shows the temporal variation of abundances and $^{12}\text{C}/^{13}\text{C}$ ratios of some selected species in the static phase without the direct C-atom

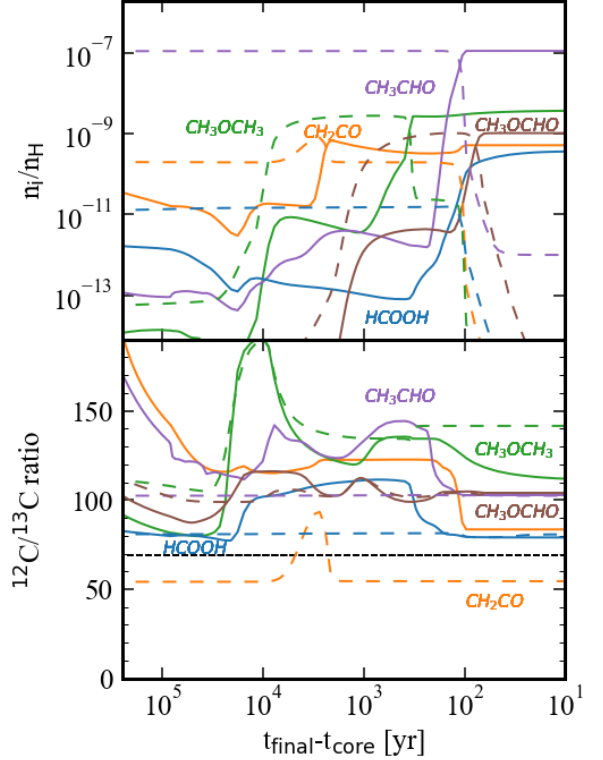


Figure 7. Same as right panel of Figure 3 but adopting the direct C-atom addition reactions and initial $^{12}\text{C}/^{13}\text{C} = 89$. The horizontal black dotted line in the lower panel represents the average $^{12}\text{C}/^{13}\text{C}$ ratio of the Solar System.

addition reactions in this case. The abundance of C^+ is half of that in the base model, so the abundances of molecules formed from C^+ such as CH_4 become smaller compared to the base model, and their $^{12}\text{C}/^{13}\text{C}$ ratios become significantly elevated compared to the base model. For example, around 10^6 yr in the static phase, the abundance of CH_4 ice is 1.0×10^{-5} , that is about 2 times smaller and the $^{12}\text{C}/^{13}\text{C}$ ratio of CH_4 is around 210, that is about 1.5 times larger compared to those in the base model, in which the abundance is 2.1×10^{-5} and the ratio is 124. On the other hand, CO is more abundant than in the base model, but as shown in the base model (see left panel of Fig.2) almost carbon eventually transforms into CO at 10^6 yr in the static phase. Therefore, the effect of initial carbon form on the molecules formed from CO is smaller than that on the molecules formed from C^+ . Around 10^6 yr in the static phase, the abundance of CH_3OH ice is 3.0×10^{-5} and the $^{12}\text{C}/^{13}\text{C}$ ratio of CH_3OH is 60, those values are similar to those in the base model, in which the abundance is 3.7×10^{-5} and the ratio is 59. Some complex molecules formed from both ^{13}C -poor and ^{13}C -rich species via radical-radical reactions or the direct C-atom addition reactions are not significantly affected by an ini-

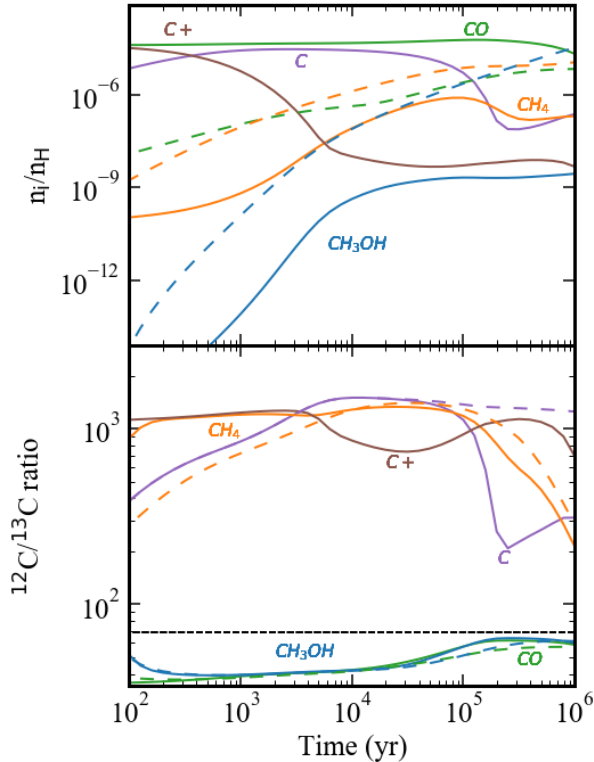


Figure 8. Same as left panel of Figure 2 but with the initial condition in which half of the carbon is in the form of CO, while the remaining half is in the form of C⁺

tial form of carbon. However, complex molecules mainly formed from ¹³C-poor species such as C₃H₄ show depletion in ¹³C compared to the base model. Therefore, if we consider these molecules, we need to account for the influence of the initial form of carbon on the carbon isotope ratios.

4. DISCUSSION

4.1. Discussion of Individual Species

4.1.1. CH₂CO

In our base model, CH₂CO gas is depleted in ¹³C, and ¹²C/¹³C ~ 95 after water ice sublimation (Fig. 3). This value is set by the sublimation of CH₂CO ice. CH₂CO ice is mainly formed from C₂ ice on the grain surface via a reaction with atomic O followed by a sequence of hydrogen addition reactions on the grain surfaces in early time ($t_{\text{final}} - t_{\text{core}} \sim 10^4$ yr) of the collapse phase. C₂ ice is mainly formed from C₂H₂ ice or via the adsorption of gaseous C₂, which become depleted in ¹³C (¹²C/¹³C ~ 100) due to the reaction in Eq.(1), around 10⁶ yr in the static phase. Therefore, the ¹²C/¹³C ratio of sublimated CH₂CO is depleted in ¹³C as well. In the model with the direct C-atom addition reactions, the formation of CH₂CO ice is much more efficient in the static phase

compared to the base model. CH₂CO ice is formed from C₂O ice on the grain surface via a sequence of hydrogen addition reactions. C₂O ice is formed by the direct C-atom addition reaction, Eq.(3). So, the ice is enriched in ¹³C as well as CO ice (¹²C/¹³C ~ 50). Additionally, ¹³C-depleted CH₂CO ice is also formed in the collapse phase as in the base model. At the CH₂CO sublimation temperature (~ 40 K, $t_{\text{final}} - t_{\text{core}} \sim 2 \times 10^3$ yr), the CH₂CO ice on the grain surface are desorbed into the gas phase and CH₂CO gas becomes depleted in ¹³C. At water sublimation temperature (~ 120 K, $t_{\text{final}} - t_{\text{core}} \sim 10^2$ yr), CH₂CO ice in the mantle phase, which is mainly formed in the static phase and enriched in ¹³C, is evaporated into the gas phase and CH₂CO gas eventually turned into slightly enriched in ¹³C (¹²C/¹³C = 64, Fig. A2).

4.1.2. CH₃CHO

Our base model shows that the ¹²C/¹³C ratio of sublimated CH₃CHO is significantly depleted in ¹³C (¹²C/¹³C ~ 132). CH₃CHO ice is formed from ¹³C-depleted C⁺ and atomic C before 10⁵ yr in the static phase as shown in Fig. 5. In addition, in early time ($t_{\text{final}} - t_{\text{core}} \sim 10^3$ yr, Fig. 2) of the collapse phase, CH₃CHO ice is formed from CH₂CO ice via a sequence of hydrogenation reactions or a radical-radical reaction between CH₃ and HCO on the grain surfaces. These reactants are slightly depleted in ¹³C (¹²C/¹³C ~ 100). Therefore, sublimated CH₃CHO has lower ¹²C/¹³C ratio compared to the CH₃CHO ice formed in the static phase (Fig. 3). In the model with the direct C-atom addition reactions, CH₃CHO ice is mainly formed in the static phase due to the direct C-atom addition reaction, Eq.(3), and has lower ¹²C/¹³C ratio compared to the base model without the direct C-atom addition reactions (see Section 3.2). Unlike CH₂CO, CH₃CHO ice mainly formed in the static phase, so the ¹²C/¹³C ratio of sublimated CH₃CHO is equal to that of CH₃CHO ice which is formed in the static phase and has lower ¹²C/¹³C ratio compared to the base model without the direct C-atom addition reactions. Therefore, the direct C-atom addition reactions decrease the ¹²C/¹³C ratio of CH₃CHO to ~ 80.

In this work, we introduced two hydrogenation reactions on grain surfaces; CH₂CO ice + H ice → CH₃CO ice and CH₃CO ice + H ice → CH₃CHO ice, following Ruaud et al. (2015). The hydrogen addition to CH₂CO ice is the dominant pathway for CH₃CHO ice formation. This pathway also plays an important role in keeping low carbon isotope ratio of CH₃CHO in the direct C-atom addition model since C₂O is formed from ¹³C-enriched CO and then the subsequent hydrogenation reactions of

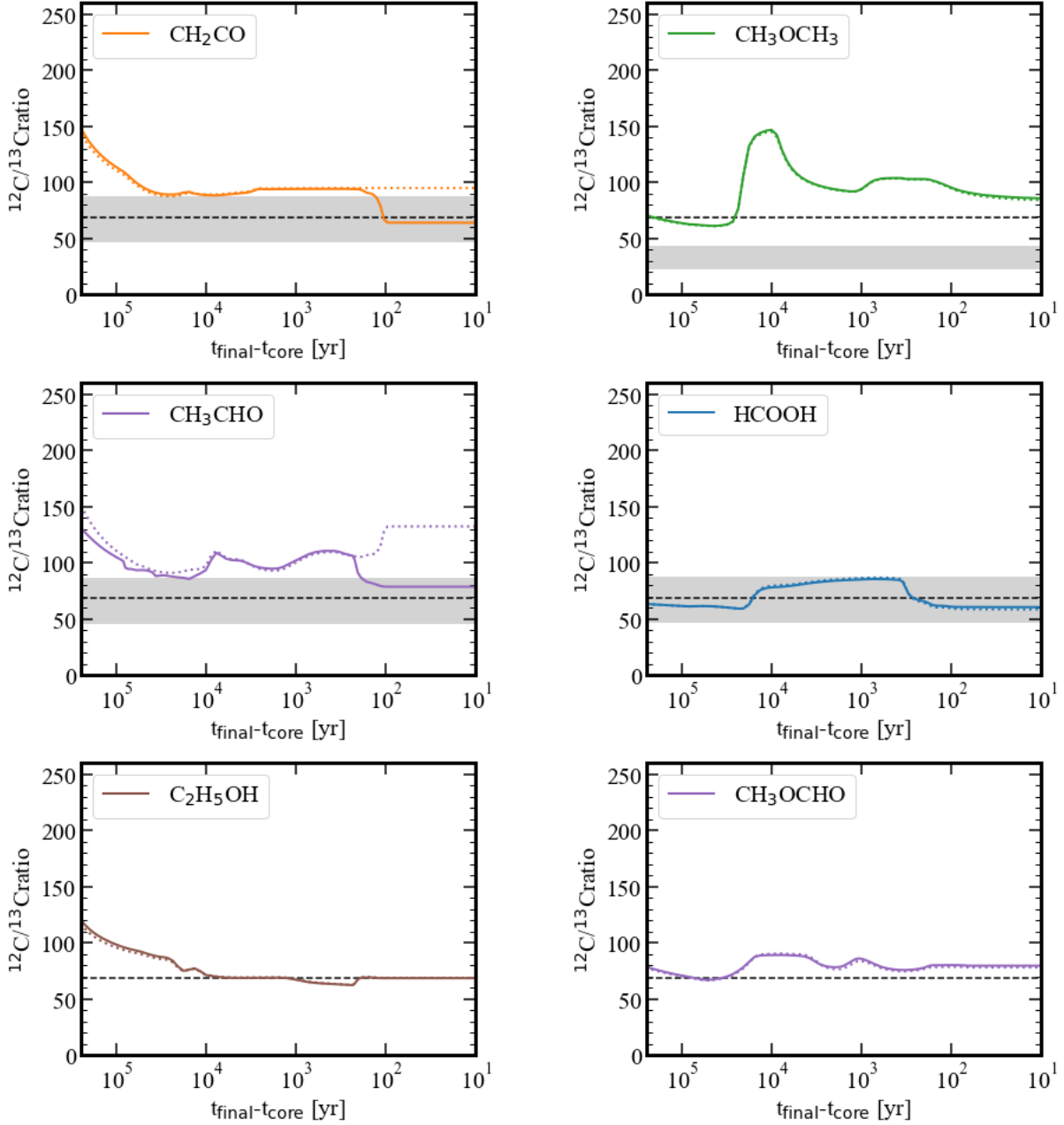


Figure 9. Temporal variation of $^{12}\text{C}/^{13}\text{C}$ ratios of some organic molecules for the base model (dotted lines) and the model with the direct C-atom addition reactions (solid lines). The black horizontal dashed line is for the average $^{12}\text{C}/^{13}\text{C}$ ratio of local ISM. The observations in IRAS16293-2422B are represented in light gray shaded regions. The observations of $\text{C}_2\text{H}_5\text{OH}$ and CH_3OCHO have large uncertainties, so we refrain from comparing our results with the observations.

C_2O on the grain surfaces forms CH_3CHO . Without this hydrogenation pathway of CH_2CO , the $^{12}\text{C}/^{13}\text{C}$ ratio of CH_3CHO gas is significantly depleted in ^{13}C ($^{12}\text{C}/^{13}\text{C} \sim 120$) after water is sublimated even though we incorporate the direct C-atom addition reactions.

4.1.3. CH_3OCH_3

In our base model, CH_3OCH_3 ice is mainly formed in the collapse phase from ^{13}C -poor CH_3 and ^{13}C -rich

CH_3O radical, so the $^{12}\text{C}/^{13}\text{C}$ ratio of CH_3OCH_3 ice is intermediate value, ~ 100 before the sublimation. In addition, CH_3OCH_3 is formed in the hot gas phase via proton transfer. The gaseous CH_3OCH_3 is formed from the reaction between CH_3OH and CH_3OH_2^+ via proton transfer. The $^{12}\text{C}/^{13}\text{C}$ ratio gradually gets close to that of CH_3OH after the sublimation, and decreases to ~ 85 . In the model with the direct C-atom addition reactions, the $^{12}\text{C}/^{13}\text{C}$ ratio of CH_3OCH_3 is similar to that in the

Table 1. $^{12}\text{C}/^{13}\text{C}$ ratio for some organic molecules in IRAS16293-2422B and our modeling results.

Species	Observation ^a	Base Model ^b	C-atom Addition ^b
CH ₂ CO	68 ± 20 ^c	95	64
CH ₃ CHO	67 ± 20	132	78
HCOOH	68 ± 20 ^c	58	60
CH ₃ OCH ₃	34 ± 10	85	86

^(a) Jørgensen et al. (2018). The uncertainties on the ratios are 30% from error propagation of the noise in the observations. ^(b) carbon isotope ratios of gas-phase molecules at 30.6 au from the core center in our models are listed. ^(c) The ISM value is used, which is consistent with the carbon isotope ratios derived using a few optically thin lines of main isotopologues of CH₂CO and HCOOH.

base model because CH₃OCH₃ is mostly formed during the collapse phase and the $^{12}\text{C}/^{13}\text{C}$ ratio changes with time. Both in the models with and without the direct C-atom addition reactions, CH₃OCH₃ remains depleted in ^{13}C after water ice is sublimated.

4.1.4. HCOOH

In our base model, HCOOH ice is formed from CO in the static phase, so the ice is slightly enriched in ^{13}C (by $\sim 10\%$) at $t_{\text{core}} \sim t_{\text{final}}$. The $^{12}\text{C}/^{13}\text{C}$ ratio of sublimated HCOOH is also slightly enriched in ^{13}C . After the sublimation gaseous HCOOH is additionally formed from H₂CO, which originates from CO, via OH + H₂CO → HCOOH. Thus, the $^{12}\text{C}/^{13}\text{C}$ ratio of HCOOH doesn't change and remains close to that of CO. In the model with the direct C-atom addition reactions, the $^{12}\text{C}/^{13}\text{C}$ ratio of HCOOH is similar to that in the base model since HCOOH ice is mainly formed from CO during the later static phase ($\sim 10^5$ yr).

4.1.5. C₂H₅OH

In our model, the $^{12}\text{C}/^{13}\text{C}$ ratio of C₂H₅OH gas is ~ 69 after water ice sublimation. This value is set by the sublimation of C₂H₅OH ice which is mainly formed via radical-radical reaction on the grain surface during the collapse phase. The formation of C₂H₅OH ice involves the reaction between ^{13}C -poor CH₃ ice and slightly ^{13}C -rich CH₂OH ice. As a result, the $^{12}\text{C}/^{13}\text{C}$ ratio of C₂H₅OH aligns with the local ISM value. This remains the case even after including the direct C-atom addition reactions.

4.1.6. CH₃OCHO

In our model, the $^{12}\text{C}/^{13}\text{C}$ ratio of CH₃OCHO gas is ~ 79 after water ice sublimation. This value is set by the sublimation of CH₃OCHO ice which is mainly formed via radical-radical reaction on the grain surface during the collapse phase. CH₃OCHO ice is formed via radical-radical reaction between ^{13}C -poor CH₃O ice and ^{13}C -rich HCO ice, so the $^{12}\text{C}/^{13}\text{C}$ ratio of CH₃OCHO is

intermediate value (=80) regardless of the direct C-atom addition reactions.

4.2. Comparisons with Observations of IRAS16293-2422B

IRAS 16293-2422B is a low-mass protostar harboring a hot corino. Icy grains accrete towards the central hot region surrounding the protostar, and the bulk water ice sublimates at 100 - 200 K. As a result, the composition of the hot corino region is thought to be determined by the ice sublimation. In our model, the region where water ice sublimates, located inside approximately 100 au from the core center, is larger than the angular resolution of the PILS survey, which is a 60 au diameter. Therefore, this region is distinctly resolved. We compare our modeling results to the observational data for the IRAS 16293-2422B, which are obtained by the ALMA-PILS line surveys (Jørgensen et al. 2016, 2018).

In Figure 9 and Table 1, our results are compared with the observations. We note that the physical model adopted in our work reproduces moderately well the observations of IRAS 16293-2422 (e.g., Figure 1 of Wakelam et al. 2014). Table 1 compares the observations and the results of our calculations at $t_{\text{core}} \sim t_{\text{final}}$ for the base model and the model with the direct C-atom addition reactions. In the base model, sublimated CH₂CO, CH₃CHO, and CH₃OCH₃ are more depleted in ^{13}C than the observations while HCOOH is similar to the observations. In the model with the direct C-atom addition reactions, CH₂CO and CH₃CHO have lower $^{12}\text{C}/^{13}\text{C}$ ratios compared to those in the base model and are similar to the observational data. This suggests that the direct C-atom addition reactions could play a significant role in the formation of observed organic molecules. However, regardless of the direct C-atom addition reactions, CH₃OCH₃ remains enriched in ^{13}C and the calculated carbon isotope ratio is larger than the observation (~ 34). We need more investigation to reproduce the observed carbon isotope ratio of CH₃OCH₃.

As noted in Jørgensen et al. (2018) many of the observed lines of main isotopologues of CH_2CO and HCOOH are optically thick, so the column densities of these main isotopologues were derived from the optically thin ^{13}C isotopologues lines assuming a standard $^{12}\text{C}/^{13}\text{C}$ ratio ($= 68$). The derived column densities of CH_2CO and HCOOH are consistent with the observations of a few optically thin transition lines of main isotopologues.

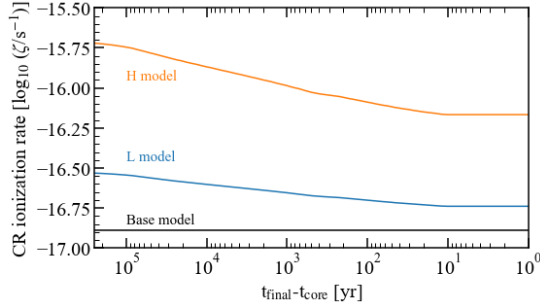


Figure 10. Temporal variation of the CR ionization rate per H_2 for the base model (black line), H model (orange line), and L model (blue line) during the collapse phase.

4.3. The Effect of Cosmic Ray

Since the calculated carbon isotope ratio of CH_3OCH_3 gas does not reproduce the observed value, we investigate the effect of cosmic ray on the $^{12}\text{C}/^{13}\text{C}$ ratio of CH_3OCH_3 and other molecules. CH_3OCH_3 gas is formed from ion-molecule reaction via proton transfer induced by cosmic-ray ionization after water ice sublimation in the collapse phase. Therefore, the $^{12}\text{C}/^{13}\text{C}$ ratio of CH_3OCH_3 can be affected by the cosmic ray ionization rate. In the models presented in previous sections, we assume that the cosmic-ray ionization rate of H_2 is constant and is $1.3 \times 10^{-17} \text{ s}^{-1}$. Here we additionally run the astrochemical models with various CR ionization rates.

4.3.1. Interstellar Cosmic Ray Flux

We adopt the CR ionization rate model as a function of gas column density in Padovani et al. (2009, 2018), in which the detailed processes of energy loss and propagation of CR are taken into account. Padovani et al. (2018) considered two models; the L (Low spectrum) model and the H (High spectrum) model for the interstellar CRs proton spectrum. L model comes from the recent data from the extrapolation of the Voyager missions (Cummings et al. 2016), while the H model is from a measurement of H_3^+ in the diffuse medium (Indriolo & McCall 2012). Figure 10 shows the temporal variation of the CR ionization rate for the model with the

constant CR ionization rate of $1.3 \times 10^{-17} \text{ s}^{-1}$, the H model, and L model. We run the chemical reaction network calculations using the H model and L model for CR ionization rate with and without the direct C-atom addition reactions.

Figure 11 shows the temporal variation of molecular abundances and $^{12}\text{C}/^{13}\text{C}$ ratios in the static phase in the H model. The higher CR ionization rate leads to the shorter timescale of ion-neutral chemical reactions including isotope exchange reactions. Gaseous CO already becomes a dominant carbon reservoir around 10^4 yr. Thus, the degree of the isotope exchange reactions decreases, and then the $^{12}\text{C}/^{13}\text{C}$ ratio of CO gets closer to the local ISM value. The molecules formed from CO, such as CH_3OH , HCOOH , and CH_3OCH_3 and ices thereof mainly after 10^5 yr, have the $^{12}\text{C}/^{13}\text{C}$ ratio closer to the local ISM value compared to those in the base model. The $^{12}\text{C}/^{13}\text{C}$ ratios of other species (e.g. CH_3CHO) and their ices formed from ^{13}C -depleted C^+ or atomic C are smaller compared to those in the base model. Around 10^6 yr higher CR ionization rate leads to atomic C being depleted in ^{13}C because ionized and atomic C is produced by secondary photons, coming from CR-induced H_2 electronic excitation and the efficiency of the isotope exchange reactions increases (Colzi et al. 2020). Therefore, the molecules formed from C^+ or atomic C, such as gaseous CH_4 also become more depleted in ^{13}C than in the base model at 10^6 yr.

Figure 12 shows the temporal variation of molecular abundances and $^{12}\text{C}/^{13}\text{C}$ ratios in the collapse phase with the H model. In the early time ($t_{\text{final}} - t_{\text{core}} \sim 10^4$ yr) some icy COMs (e.g. CH_3OCH_3) are produced more efficiently by the higher CR ionization rates, and these are depleted in ^{13}C . The CR-induced UV photons dissociate stable molecules producing radicals on grain surfaces, and then stimulate the formation of COMs on the grain surface. For example, the CH_3 ice on the grain surface is also depleted in ^{13}C since the gaseous CH_4 is depleted in ^{13}C at the end of the static phase. As a result, COMs formed from CH_3 ice by radical-radical reactions on warm grains become more depleted in ^{13}C after water ice sublimation than in the base model. Moreover, for a higher CR ionization rate, the $^{12}\text{C}/^{13}\text{C}$ ratio of CH_3OCH_3 gas approaches that of CH_3OH more quickly, because the CR ionization rate promotes the formation of $\text{CH}_3\text{OCH}_4^+$ via ion-molecule reactions and then the formation of CH_3OCH_3 by the following dissociative recombination, $\text{CH}_3\text{OCH}_4^+ + \text{e}^- \rightarrow \text{CH}_3\text{OCH}_3$ form CH_3OCH_3 in the warm gas phase. However, the $^{12}\text{C}/^{13}\text{C}$ ratio of CH_3OCH_3 at $t_{\text{core}} \sim t_{\text{final}}$ is ~ 100 , which is higher than that in the base model (see Figure. 2) because the $^{12}\text{C}/^{13}\text{C}$ ratio of CH_3OCH_3 after water

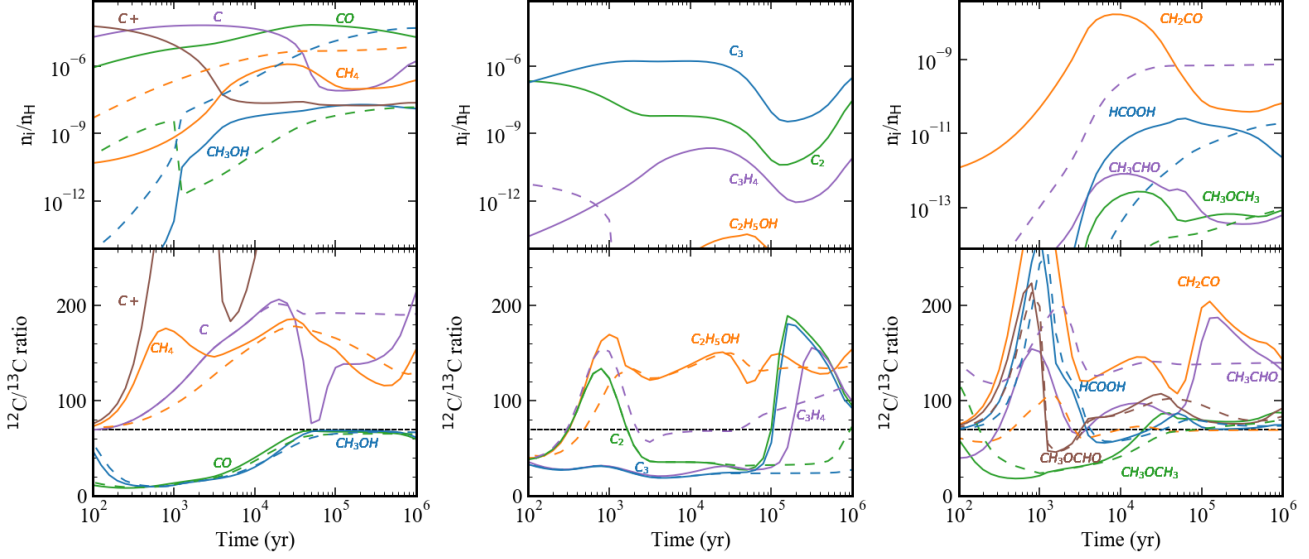


Figure 11. Same as Figure 2 but for the H model for CR ionization rate

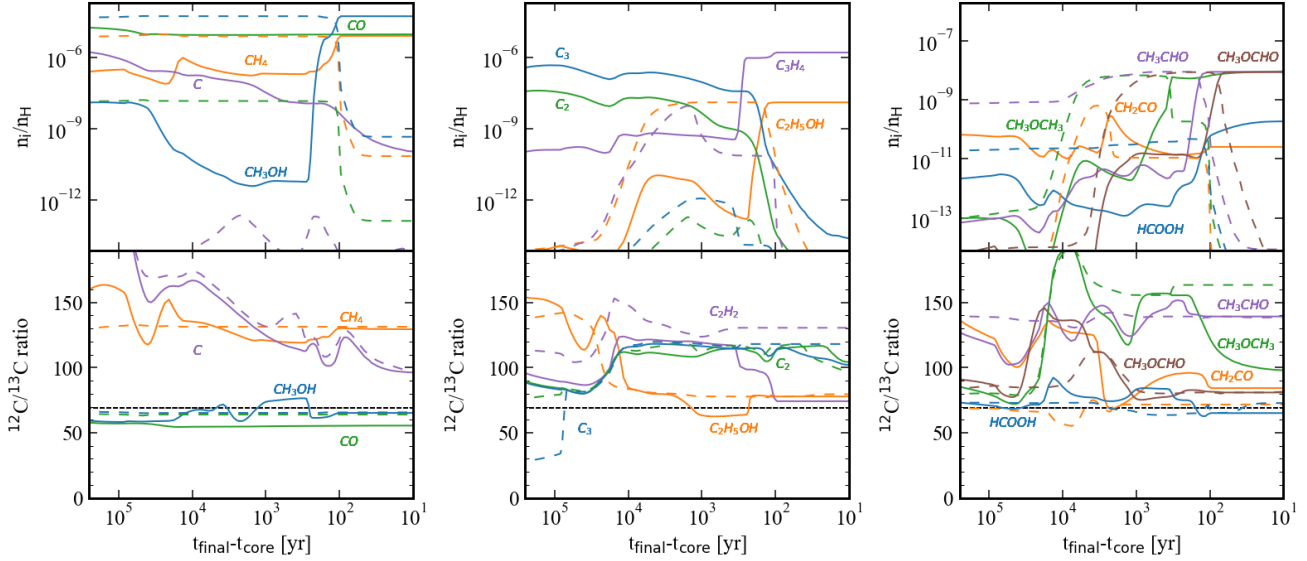


Figure 12. Same as Figure 3 but for the H model for CR ionization rate

ice sublimation is significantly depleted in ^{13}C ($^{12}\text{C}/^{13}\text{C} \sim 160$).

We incorporate the direct C-atom addition reactions together with the H model. Figure 13 shows the temporal variation of molecular abundances and $^{12}\text{C}/^{13}\text{C}$ ratios in the collapse phase with the H model and the direct C-atom addition reactions. In the H model, the suppression of $^{12}\text{C}/^{13}\text{C}$ ratios of COMs (e.g. CH_3CHO) does not occur even when considering the direct C-atom addition reactions. Atomic C becomes CO and is depleted in the gas phase at $\sim 10^4$ yr in the static phase, so the degree of the direct C-atom addition reactions become smaller, and the abundances of icy COMs produced via the direct C-atom addition reactions in the

static phase becomes smaller compared to the model with the constant CR ionization rate of $1.3 \times 10^{-17} \text{ s}^{-1}$ and the direct C-atom addition reactions. These icy COMs are much more formed via radical-radical reactions in the collapse phase in the same as the model without the direct C-atom addition reactions. As a result, the $^{12}\text{C}/^{13}\text{C}$ ratios of COMs in the warm gas trace those formed on warm dust grains during the collapse phase. For example, the abundance of CH_3CHO ice at 10^6 yr in the static phase decreases by a factor of 100 (the molecular abundance is $\sim 10^{-9}$) (see also Figure 4). On the other hand, the abundance of CH_3CHO ice formed from ^{13}C -depleted CH_3 during the collapse phase is ten times larger than that formed in the static phase.

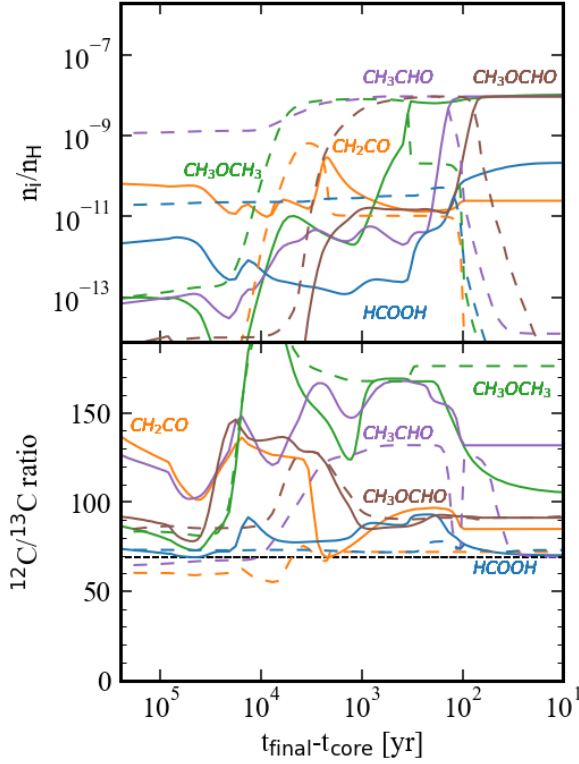


Figure 13. Same as right panel of Figure 3 but adopting the H model for CR ionization rate and the direct C-atom addition reactions.

As a result, the $^{12}\text{C}/^{13}\text{C}$ ratio of CH_3CHO gas after water ice sublimation is depleted in ^{13}C despite incorporating the direct C-atom addition reactions. Therefore, the high CR ionization rate during the static phase is not suitable for the formation of COMs (such as CH_3CHO) in the viewpoint of their carbon isotope ratios. For the L model, the result is similar to that of the model with the constant CR ionization rate of $1.3 \times 10^{-17} \text{ s}^{-1}$.

4.3.2. Cosmic Ray Acceleration after protostar formation

Following the results in Sect. 4.3.1, in this section, we consider the effect of possible variations of CR ionization rate during the star formation. CRs are suggested to be accelerated by the local shocks around the protostar (Padovani et al. 2015, 2016) such as strongly magnetized shock along the outflow or by the accretion shocks. Cabedo et al. (2023) measured abundances of molecular ions in a solar-type protostellar object and suggest high CR ionization rates of $10^{-16} - 10^{-14} \text{ s}^{-1}$, possibly locally accelerated at shocks. We run the additional model in which we set the CR ionization rate to be $1.3 \times 10^{-14} \text{ s}^{-1}$ after the protostellar formation. We note that the CR ionization rate higher than $1.3 \times 10^{-14} \text{ s}^{-1}$ destroys COMs via proton transfer by H_3O^+ after sublimation as suggested by Nomura & Millar (2004) and

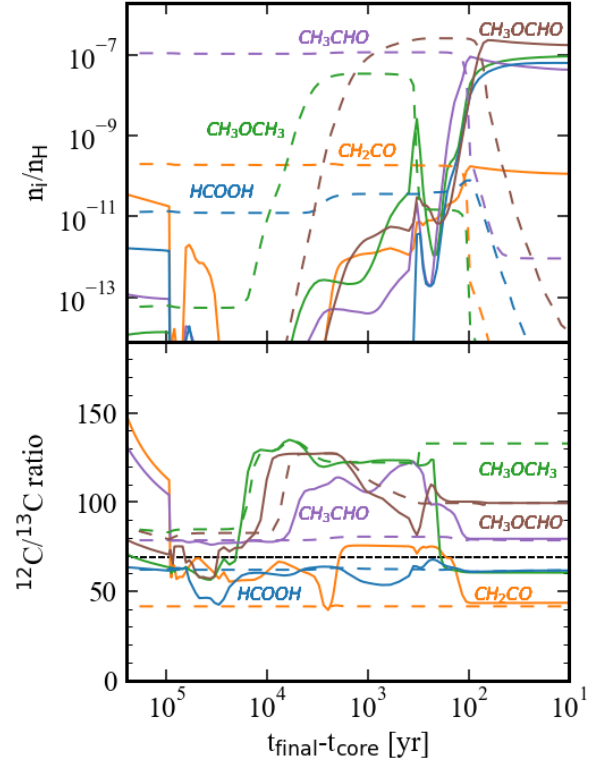


Figure 14. Same as right panel of Figure 3 but with the direct C-atom addition reactions, and $1.3 \times 10^{-14} \text{ s}^{-1}$ as CR ionization rate after the protostar birth.

eventually abundance of some molecules (e.g. CH_3CHO and CH_3OCH_3) decrease to around 1×10^{-11} at $t_{\text{core}} = t_{\text{final}}$. Figure 14 shows the temporal variation of molecular abundances and $^{12}\text{C}/^{13}\text{C}$ ratios in the collapse phase with CR ionization rate of $1.3 \times 10^{-14} \text{ s}^{-1}$ and the direct C-atom addition reactions. CH_3OCH_3 is formed from CH_3OH and CH_3OH_2^+ via proton transfer after water ice sublimation and then the $^{12}\text{C}/^{13}\text{C}$ ratio of CH_3OCH_3 approaches that of CH_3OH and becomes enriched in ^{13}C (~ 60). Consequently, the $^{12}\text{C}/^{13}\text{C}$ ratio of CH_3OCH_3 decreases if the CR ionization rates become high only in the collapse phase. However, the ratio is still higher than the observation towards IRAS16293-2422B (Jørgensen et al. 2018). For other selected molecules, the $^{12}\text{C}/^{13}\text{C}$ ratios of HCOOH and CH_3CHO are similar to those in the base model with the direct C-atom addition reactions (see a right panel of Fig. A2). The $^{12}\text{C}/^{13}\text{C}$ ratio of CH_2CO , on the other hand, reflects enrichment of ^{13}C in the CH_2CO ice formed in the static phase unlike that in the model with constant CR ionization rate of $1.3 \times 10^{-14} \text{ s}^{-1}$ and the direct C-atom addition reactions. In the case of a high CR ionization rate, CH_2CO ice is not formed during the collapse phase, so the $^{12}\text{C}/^{13}\text{C}$ ratio of sublimated CH_2CO is similar to that of CH_2CO ice formed in the static phase.

5. SUMMARY

We investigated the carbon isotope fractionation of COMs from prestellar cores to protostellar cores by combining the chemical network model and the radiation hydrodynamical simulation. The temporal variation of the molecular abundances and $^{12}\text{C}/^{13}\text{C}$ ratios were calculated by conducting calculations of a gas-grain chemical network within a single fluid parcel. Our main findings are the following.

1. In the static prestellar phase, due to the carbon isotope exchange reactions, the molecules formed from atomic C and C^+ were depleted in ^{13}C , while the molecules formed from CO were around 10 % enriched in ^{13}C at the end of the static phase. COMs have various $^{12}\text{C}/^{13}\text{C}$ ratios depending on the $^{12}\text{C}/^{13}\text{C}$ ratios of their reactants.
2. In the collapse phase, after the protostar formation where species are sublimated to the gas phase, the $^{12}\text{C}/^{13}\text{C}$ ratios of some sublimated species (e.g. CH_4 and CH_3OH) reflected those of their icy counterparts. On the other hand, the $^{12}\text{C}/^{13}\text{C}$ ratios of other species are affected by chemical reactions during the collapse phase. Some COMs (e.g. CH_3CHO) were formed on warm grain surfaces during the collapse phase as much as in the static phase. As a result, the $^{12}\text{C}/^{13}\text{C}$ ratios of these COMs were different from those of their icy counterparts formed in the static phase. In addition, some COMs (e.g. CH_3OCH_3) were formed in the warm gas phase after water ice sublimation, which also affects their carbon isotope ratios. Eventually, in our base model, some complex molecules (e.g. CH_3CHO and CH_3OCH_3) become more depleted in ^{13}C compared to the observations.
3. We incorporated the direct C-atom addition reactions into our base model and investigated the

effect of these reactions on the formation and the $^{12}\text{C}/^{13}\text{C}$ ratios of COMs. Direct C-atom addition reactions altered the $^{12}\text{C}/^{13}\text{C}$ ratios of molecules, reducing the diversity of the carbon isotope ratios. This is due to the additional formation of specific species (e.g., H_2CO and C_2O), which further lead to the production of COMs. Our results reproduced the observations of the $^{12}\text{C}/^{13}\text{C}$ ratios of some complex molecules including COMs (CH_2CO , CH_3CHO , and HCOOH) in the Class 0 source, IRAS16293-2422B, which were comparable to the elemental $^{12}\text{C}/^{13}\text{C}$ ratio in the local ISM. However, CH_3OCH_3 in our results still shows depletion of ^{13}C compared to the observations.

4. We investigated the effect of various CR ionization rates on carbon isotope ratios of complex molecules. During the static phase, high cosmic ray (CR) ionization rates are considered unfavorable for the formation of complex organic molecules (COMs). Consequently, the formation of ^{13}C -rich COMs through direct C-atom addition reactions becomes less efficient. Instead, ^{13}C -depleted radicals, such as CH_3 , tend to form COMs on warm grain surfaces during the collapse phase. On the other hand, ion-molecule reactions in the warm gas phase reduced the $^{12}\text{C}/^{13}\text{C}$ ratio of CH_3OCH_3 after water ice sublimation. Especially, when the CR ionization rates become as high as $1.3 \times 10^{-14} \text{ s}^{-1}$ only after protostar formation, this ratio becomes enriched in ^{13}C . However, the $^{12}\text{C}/^{13}\text{C}$ ratio of CH_3OCH_3 at the end of the collapse phase was still higher than the observations.

We thank the anonymous referees for the helpful comments to improve the manuscript. This work is supported by JSPS and MEXT Grants-in-Aid for Scientific Research, 18H05441, 19K03910, 20H00182 (H.N.).

REFERENCES

- Agúndez, M., Cernicharo, J., & Guélin, M. 2015, *A&A*, 577, L5, doi: [10.1051/0004-6361/201526317](https://doi.org/10.1051/0004-6361/201526317)
- Aikawa, Y., Furuya, K., Yamamoto, S., & Sakai, N. 2020, *ApJ*, 897, 110, doi: [10.3847/1538-4357/ab994a](https://doi.org/10.3847/1538-4357/ab994a)
- Aikawa, Y., Ohashi, N., Inutsuka, S.-i., Herbst, E., & Takakuwa, S. 2001, *ApJ*, 552, 639, doi: [10.1086/320551](https://doi.org/10.1086/320551)
- Aikawa, Y., Wakelam, V., Garrod, R. T., & Herbst, E. 2008, *ApJ*, 674, 984, doi: [10.1086/524096](https://doi.org/10.1086/524096)
- Cabedo, V., Maury, A., Girart, J. M., et al. 2023, *A&A*, 669, A90, doi: [10.1051/0004-6361/202243813](https://doi.org/10.1051/0004-6361/202243813)
- Colzi, L., Sipilä, O., Roueff, E., Caselli, P., & Fontani, F. 2020, *A&A*, 640, A51, doi: [10.1051/0004-6361/202038251](https://doi.org/10.1051/0004-6361/202038251)
- Cummings, A. C., Stone, E. C., Heikkilä, B. C., et al. 2016, *ApJ*, 831, 18, doi: [10.3847/0004-637X/831/1/18](https://doi.org/10.3847/0004-637X/831/1/18)
- Fedoseev, G., Qasim, D., Chuang, K.-J., et al. 2022, *ApJ*, 924, 110, doi: [10.3847/1538-4357/ac3834](https://doi.org/10.3847/1538-4357/ac3834)

- Ferrero, S., Ceccarelli, C., Ugliengo, P., Sodupe, M., & Rimola, A. 2023, *ApJ*, 951, 150, doi: [10.3847/1538-4357/acd192](https://doi.org/10.3847/1538-4357/acd192)
- . 2024, *ApJ*, 960, 22, doi: [10.3847/1538-4357/ad0547](https://doi.org/10.3847/1538-4357/ad0547)
- Furuya, K., Aikawa, Y., Hincelin, U., et al. 2015, *A&A*, 584, A124, doi: [10.1051/0004-6361/201527050](https://doi.org/10.1051/0004-6361/201527050)
- Furuya, K., Aikawa, Y., Sakai, N., & Yamamoto, S. 2011, *ApJ*, 731, 38, doi: [10.1088/0004-637X/731/1/38](https://doi.org/10.1088/0004-637X/731/1/38)
- Furuya, K., van Dishoeck, E. F., & Aikawa, Y. 2016, *A&A*, 586, A127, doi: [10.1051/0004-6361/201527579](https://doi.org/10.1051/0004-6361/201527579)
- Garrod, R. T. 2013, *ApJ*, 765, 60, doi: [10.1088/0004-637X/765/1/60](https://doi.org/10.1088/0004-637X/765/1/60)
- Garrod, R. T., & Herbst, E. 2006, *A&A*, 457, 927, doi: [10.1051/0004-6361:20065560](https://doi.org/10.1051/0004-6361:20065560)
- Garrod, R. T., Jin, M., Matis, K. A., et al. 2022, *ApJS*, 259, 1, doi: [10.3847/1538-4365/ac3131](https://doi.org/10.3847/1538-4365/ac3131)
- Hasegawa, T. I., & Herbst, E. 1993, *MNRAS*, 263, 589, doi: [10.1093/mnras/263.3.589](https://doi.org/10.1093/mnras/263.3.589)
- Herbst, E., & van Dishoeck, E. F. 2009, *ARA&A*, 47, 427, doi: [10.1146/annurev-astro-082708-101654](https://doi.org/10.1146/annurev-astro-082708-101654)
- Hollenbach, D., & McKee, C. F. 1979, *ApJS*, 41, 555, doi: [10.1086/190631](https://doi.org/10.1086/190631)
- Indriolo, N., & McCall, B. J. 2012, *ApJ*, 745, 91, doi: [10.1088/0004-637X/745/1/91](https://doi.org/10.1088/0004-637X/745/1/91)
- Jin, M., & Garrod, R. T. 2020, *ApJS*, 249, 26, doi: [10.3847/1538-4365/ab9ec8](https://doi.org/10.3847/1538-4365/ab9ec8)
- Jørgensen, J. K., van der Wiel, M. H. D., Coutens, A., et al. 2016, *A&A*, 595, A117, doi: [10.1051/0004-6361/201628648](https://doi.org/10.1051/0004-6361/201628648)
- Jørgensen, J. K., Müller, H. S. P., Calcutt, H., et al. 2018, *A&A*, 620, A170, doi: [10.1051/0004-6361/201731667](https://doi.org/10.1051/0004-6361/201731667)
- Langer, W. D., Graedel, T. E., Frerking, M. A., & Armentrout, P. B. 1984, *ApJ*, 277, 581, doi: [10.1086/161730](https://doi.org/10.1086/161730)
- Loison, J.-C., Wakelam, V., Gratier, P., & Hickson, K. M. 2020, *MNRAS*, 498, 4663, doi: [10.1093/mnras/staa2700](https://doi.org/10.1093/mnras/staa2700)
- Manigand, S., Jørgensen, J. K., Calcutt, H., et al. 2020, *A&A*, 635, A48, doi: [10.1051/0004-6361/201936299](https://doi.org/10.1051/0004-6361/201936299)
- Masunaga, H., & Inutsuka, S.-i. 2000, *ApJ*, 531, 350, doi: [10.1086/308439](https://doi.org/10.1086/308439)
- Milam, S. N., Savage, C., Brewster, M. A., Ziurys, L. M., & Wyckoff, S. 2005, *ApJ*, 634, 1126, doi: [10.1086/497123](https://doi.org/10.1086/497123)
- Molpeceres, G., Kästner, J., Fedoseev, G., et al. 2021, *The Journal of Physical Chemistry Letters*, 12, 10854, doi: [10.1021/acs.jpcclett.1c02760](https://doi.org/10.1021/acs.jpcclett.1c02760)
- Nomura, H., & Millar, T. J. 2004, *A&A*, 414, 409, doi: [10.1051/0004-6361:20031646](https://doi.org/10.1051/0004-6361:20031646)
- Nomura, H., Furuya, K., Cordiner, M. A., et al. 2023, in *Astronomical Society of the Pacific Conference Series*, Vol. 534, *Astronomical Society of the Pacific Conference Series*, ed. S. Inutsuka, Y. Aikawa, T. Muto, K. Tomida, & M. Tamura, 1075
- Padovani, M., Galli, D., & Glassgold, A. E. 2009, *A&A*, 501, 619, doi: [10.1051/0004-6361/200911794](https://doi.org/10.1051/0004-6361/200911794)
- Padovani, M., Hennebelle, P., Marcowith, A., & Ferrière, K. 2015, *A&A*, 582, L13, doi: [10.1051/0004-6361/201526874](https://doi.org/10.1051/0004-6361/201526874)
- Padovani, M., Ivlev, A. V., Galli, D., & Caselli, P. 2018, *A&A*, 614, A111, doi: [10.1051/0004-6361/201732202](https://doi.org/10.1051/0004-6361/201732202)
- Padovani, M., Marcowith, A., Hennebelle, P., & Ferrière, K. 2016, *A&A*, 590, A8, doi: [10.1051/0004-6361/201628221](https://doi.org/10.1051/0004-6361/201628221)
- Potapov, A., Krasnokutski, S. A., Jäger, C., & Henning, T. 2021, *ApJ*, 920, 111, doi: [10.3847/1538-4357/ac1a70](https://doi.org/10.3847/1538-4357/ac1a70)
- Roueff, E., Loison, J. C., & Hickson, K. M. 2015, *A&A*, 576, A99, doi: [10.1051/0004-6361/201425113](https://doi.org/10.1051/0004-6361/201425113)
- Ruaud, M., Loison, J. C., Hickson, K. M., et al. 2015, *MNRAS*, 447, 4004, doi: [10.1093/mnras/stu2709](https://doi.org/10.1093/mnras/stu2709)
- Shingledecker, C. N., Tennis, J., Le Gal, R., & Herbst, E. 2018, *ApJ*, 861, 20, doi: [10.3847/1538-4357/aac5ee](https://doi.org/10.3847/1538-4357/aac5ee)
- Sipilä, O., Colzi, L., Roueff, E., et al. 2023, *A&A*, 678, A120, doi: [10.1051/0004-6361/202347106](https://doi.org/10.1051/0004-6361/202347106)
- Smith, L. R., Gudipati, M. S., Smith, R. L., & Lewis, R. D. 2021, *A&A*, 656, A82, doi: [10.1051/0004-6361/202141529](https://doi.org/10.1051/0004-6361/202141529)
- Smith, R. L., Pontoppidan, K. M., Young, E. D., & Morris, M. R. 2015, *ApJ*, 813, 120, doi: [10.1088/0004-637X/813/2/120](https://doi.org/10.1088/0004-637X/813/2/120)
- Terzieva, R., & Herbst, E. 1998, *ApJ*, 501, 207, doi: [10.1086/305811](https://doi.org/10.1086/305811)
- Tsuge, M., Molpeceres, G., Aikawa, Y., & Watanabe, N. 2023, *Nature Astronomy*, 7, 1351, doi: [10.1038/s41550-023-02071-0](https://doi.org/10.1038/s41550-023-02071-0)
- van Dishoeck, E. F., & Black, J. H. 1988, *ApJ*, 334, 771, doi: [10.1086/166877](https://doi.org/10.1086/166877)
- Visser, R., van Dishoeck, E. F., & Black, J. H. 2009, *A&A*, 503, 323, doi: [10.1051/0004-6361/200912129](https://doi.org/10.1051/0004-6361/200912129)
- Wakelam, V., Vastel, C., Aikawa, Y., et al. 2014, *MNRAS*, 445, 2854, doi: [10.1093/mnras/stu1920](https://doi.org/10.1093/mnras/stu1920)
- Watson, W. D., Anicich, V. G., & Huntress, W. T., J. 1976, *ApJL*, 205, L165, doi: [10.1086/182115](https://doi.org/10.1086/182115)
- Yamato, Y., Notsu, S., Aikawa, Y., et al. 2024, *AJ*, 167, 66, doi: [10.3847/1538-3881/ad11d9](https://doi.org/10.3847/1538-3881/ad11d9)

APPENDIX

A. REVIEW OF CARBON ISOTOPE EXCHANGE REACTIONS INCLUDED IN THE MODEL

In table A1, we list carbon isotope exchange reactions used in our model.

Table A1. Review of carbon isotope exchange reactions included in the model

Reaction	Rate Coefficient	ΔE (K)	References
$^{13}\text{C}^+ + \text{CO} \rightleftharpoons \text{C}^+ + ^{13}\text{CO}$	$6.6 \times 10^{-10} \times \left(\frac{T}{300}\right)^{-0.45}$	34.5	(1)
$^{13}\text{CO} + \text{HCO}^+ \rightleftharpoons \text{CO} + \text{H}^{13}\text{CO}^+$	$2.6 \times 10^{-10} \times \left(\frac{T}{300}\right)^{-0.33}$	17.4	(1)
$^{13}\text{C}^+ + \text{C}_2 \rightleftharpoons \text{C}^+ + ^{13}\text{CC}$	1.86×10^{-9}	26.4	(2)
$^{13}\text{C}^+ + \text{C}_3 \rightleftharpoons \text{C}^+ + ^{13}\text{CC}_2$	1.8×10^{-9}	28.0	(2)
$^{13}\text{C}^+ + \text{CN} \rightleftharpoons \text{C}^+ + ^{13}\text{CN}$	$3.82 \times 10^{-9} \times \left(\frac{T}{300}\right)^{-0.4}$	31.1	(1)
$^{13}\text{C}^+ + \text{CS} \rightleftharpoons \text{C}^+ + ^{13}\text{CS}$	$2.0 \times 10^{-9} \times \left(\frac{T}{300}\right)^{-0.4}$	26.3	(2)
$^{13}\text{C} + \text{H}_2\text{CN}^+ \rightleftharpoons \text{C} + \text{H}_2^{13}\text{CN}^+$	1.0×10^{-9}	50.0	(2)
$\text{H}_2^{13}\text{CN}^+ + \text{HCN} \rightleftharpoons \text{H}_2\text{CN}^+ + \text{H}^{13}\text{CN}$	$2.0 \times 10^{-9} \times \left(\frac{T}{300}\right)^{-0.5}$	2.9	(2)
$\text{H}_2\text{CN}^+ + \text{HN}^{13}\text{C} \rightleftharpoons \text{H}_2^{13}\text{CN}^+ + \text{HCN}$	$1.0 \times 10^{-9} \times \left(\frac{T}{300}\right)^{-0.5}$	0	(2)
$\text{H}_2\text{CN}^+ + \text{HN}^{13}\text{C} \rightleftharpoons \text{H}_2\text{CN}^+ + \text{H}^{13}\text{CN}$	$1.0 \times 10^{-9} \times \left(\frac{T}{300}\right)^{-0.5}$	0	(2)
$^{13}\text{C} + \text{C}_2 \rightleftharpoons \text{C} + ^{13}\text{CC}$	3.0×10^{-10}	26.4	(2)
$^{13}\text{C} + \text{C}_3 \rightleftharpoons \text{C} + ^{13}\text{CC}_2$	3.0×10^{-10}	28.0	(2)
$^{13}\text{C} + \text{CN} \rightleftharpoons \text{C} + ^{13}\text{CN}$	3.0×10^{-10}	31.1	(1)
$^{13}\text{C} + \text{HCN} \rightleftharpoons \text{C} + \text{H}^{13}\text{CN}$	2.0×10^{-10}	48.0	(2)
$^{13}\text{C} + \text{HNC} \rightleftharpoons \text{C} + \text{HN}^{13}\text{C}$	3.0×10^{-11}	33.0	(2)
$^{13}\text{C} + \text{CS} \rightleftharpoons \text{C} + ^{13}\text{CS}$	2.0×10^{-10}	26.3	(2)
$^{13}\text{C} + \text{HC}_3\text{N} \rightleftharpoons \text{C} + \text{H}^{13}\text{CC}_2\text{N}$	6.0×10^{-11}	48.3	(2)

References. (1) Roueff et al. (2015); (2) Loison et al. (2020).

B. ADDITIONAL FIGURES

B.1. Carbon- and Oxygen-bearing molecules

Figure A1 and A2 show the temporal variation of abundances and the $^{12}\text{C}/^{13}\text{C}$ ratios of some molecules with the direct C-atom addition reactions in the static phase and collapse phase, respectively.

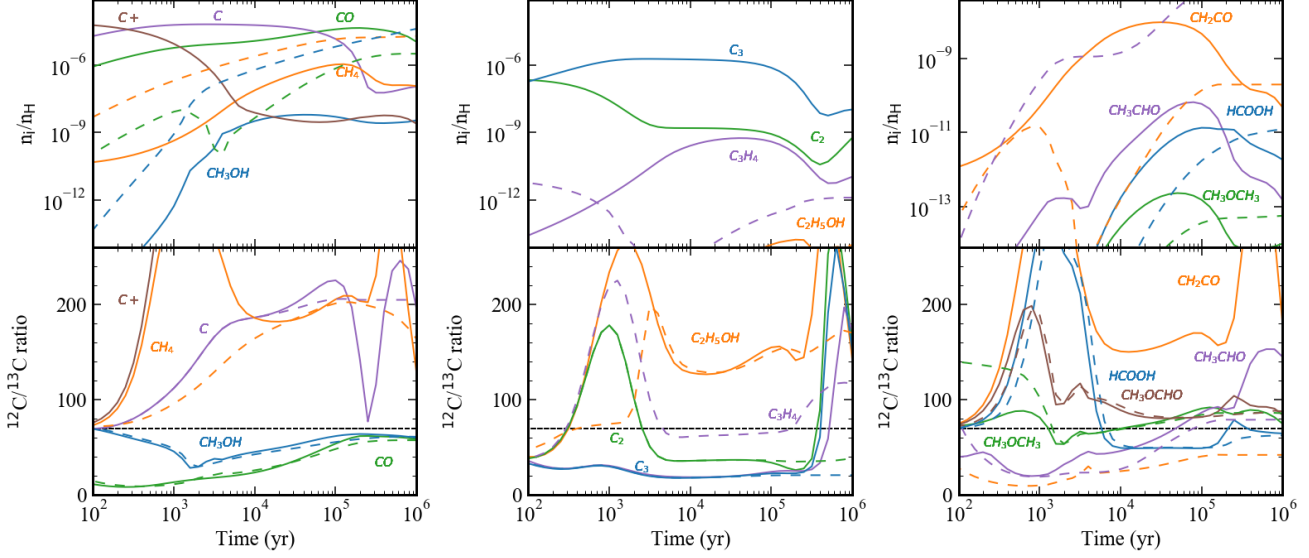


Figure A1. Same as Figure 2 but adopting the direct C-atom addition reactions

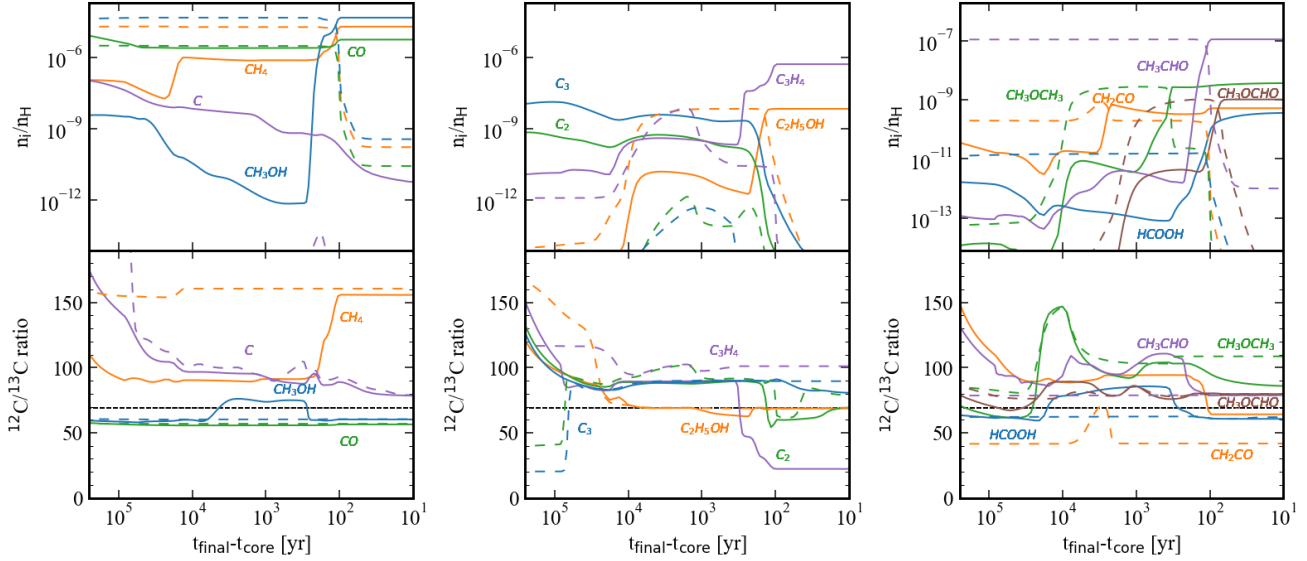


Figure A2. Same as Figure 3 but adopting the direct C-atom addition reactions.

Figure A3 shows the temporal variation of abundance and the $^{12}\text{C}/^{13}\text{C}$ ratio of HCCO gas. HCCO is formed from C_2O ice which is formed via direct C-atom addition reaction 3. Therefore, after incorporating the direct C-atom addition reactions the abundance increases, and the $^{12}\text{C}/^{13}\text{C}$ ratio decreases. HCCO was observed toward the starless core (Agúndez et al. 2015), where they reported the column density ratio of HCCO and H_2 , ranging from 10^{-13} to 10^{-11} . In our model, HCCO gas to H_2 gas ratio at typical dense cloud age ($\sim 10^5$ yr) in the static phase increases from 4.4×10^{-14} to 3.5×10^{-10} with the direct C-atom addition reaction 3. This means that HCCO gas is efficiently formed via the direct C-atom addition reaction 3 even at low-temperature environments. The $^{12}\text{C}/^{13}\text{C}$ ratio of HCCO

gas decreases from 160 to 80 at typical dense cloud age, and from 85 to 47 after water ice sublimates. Therefore, measuring the $^{12}\text{C}/^{13}\text{C}$ ratio of HCCO by observation could confirm whether the direct C-atom addition reactions contribute to forming COMs.

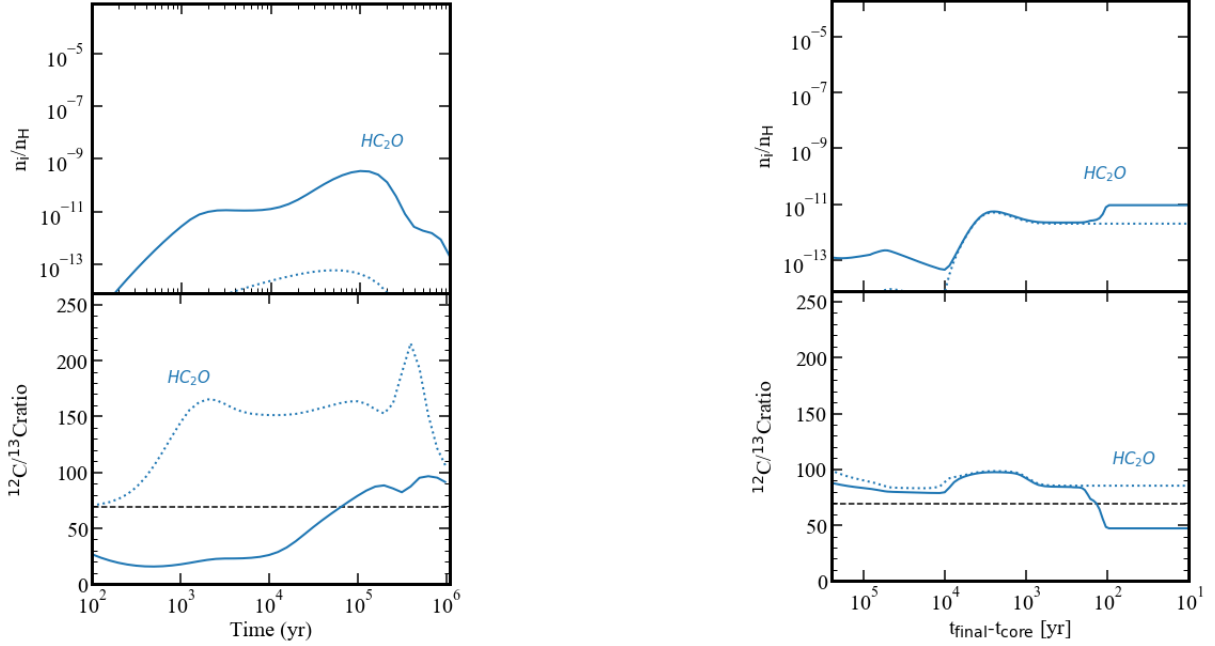


Figure A3. The temporal variation of abundance and the $^{12}\text{C}/^{13}\text{C}$ ratio of HC_2O gas for the base model (dotted lines) and the model with the direct C-atom addition reactions (solid lines). The left panel is for the static phase and the right panel is for the collapse phase.

B.2. Nitrogen-bearing molecules

Figures A4 and A5 show the temporal variation of abundances and $^{12}\text{C}/^{13}\text{C}$ ratios of nitrogen-bearing species in the static phase and the collapse phase, respectively. These results in the static phase in our model are similar to the results in Colzi et al. (2020) and Loison et al. (2020). The $^{12}\text{C}/^{13}\text{C}$ ratios are affected by carbon isotope exchange reactions. Some molecules (e.g. HNCO, H_2CN , NH_2CHO and CH_3NH) show different time variations compared to our base model at around 10^4 yr in the static phase due to the direct C-atom addition reaction 2. These molecules are formed from H_2CO ice. In the base model HNCO, H_2CN , and NH_2CHO are partly formed from ^{13}C -enriched CO and H_2CO , but in the model with the direct C-atom addition reactions H_2CO is formed via Reaction 2 and is depleted in ^{13}C , similar to atomic C. Therefore, the $^{12}\text{C}/^{13}\text{C}$ ratios of these molecules increase when the direct C-atom addition reactions are incorporated. CH_3NH is formed from CH_3 or H_2CN , so the $^{12}\text{C}/^{13}\text{C}$ ratio changes by the direct C-atom addition reactions. Around 10^6 yr, however, these differences are no longer evident because H_2CO ice is formed from CO ice via a sequence of hydrogenation reactions on the grain surface. In the collapse phase, there is no difference between our base model and the model with the direct C-atom addition reactions. For HC_3N , the $^{12}\text{C}/^{13}\text{C}$ ratio depends on the position of ^{13}C within the molecules. Therefore, we will address these aspects in future work.

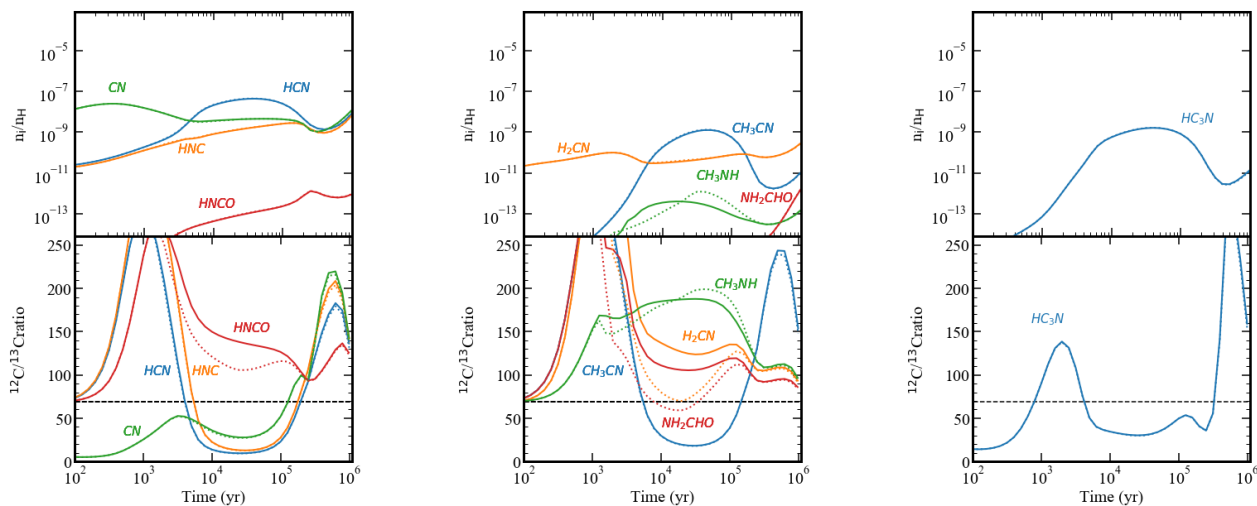


Figure A4. Temporal variation of the molecular abundances and $^{12}\text{C}/^{13}\text{C}$ ratios for gaseous species during the static phase in the model with the direct C-atom addition reactions (solid lines) and the base model (dashed lines). The horizontal black dashed line represents the average $^{12}\text{C}/^{13}\text{C}$ ratio of local ISM.

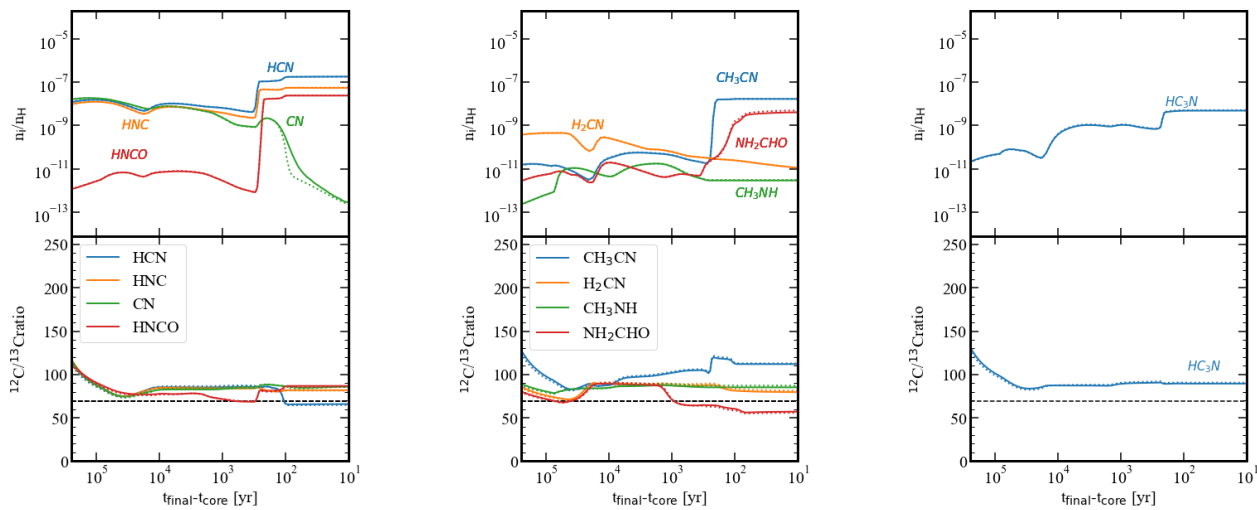


Figure A5. Same as Figure A4 but for during the collapse phase.